

AD-A278 319



~~AFOSR-TR-94-0206~~

DEPARTMENT OF COMPUTER SCIENCE
COLLEGE OF SCIENCES
OLD DOMINION UNIVERSITY
NORFOLK, VIRGINIA 23529

AFOSR-TR- 94 0206

Approved for public release;
distribution unlimited.

2

**REACTING COMPRESSIBLE MIXING LAYERS:
STRUCTURE AND STABILITY**

By

Chester Grosch, Principal Investigator

DTIC
ELECTE
APR 21 1994
S F D

Final Report
For the period October 31, 1993

Prepared for
Air Force Office of Scientific Research
Building 410/NM
Bolling AFB DC 20332

Under
Research Contract AFOSR-91-0250
Dr. Marc Q. Jacobs, Program Manager

This document has been approved
for public release and sale; its
distribution is unlimited.

5400 94-12040

October 1993

2025 RELEASE UNDER E.O. 14176

94 4 20 1 1 2

REPORT DOCUMENTATION PAGE

Form Approved
GSA No. 2704-0128

Public reporting burden for this report is estimated to average 1 hour per response, including the time for reviewing the instructions, searching existing data sources, gathering and maintaining the data needed, and completing and reviewing the collection of information. Send comments regarding this burden estimate or any other aspect of this collection of information, including suggestions for reducing this burden, to Washington Headquarters Services, Directorate for Information Operations and Reports, 1215 Jefferson Davis Highway, Suite 1204, Arlington, VA 22202-4302, and to the Office of Management and Budget, Paperwork Reduction Project (2704-0128), Washington, DC 20503.

1. AGENCY USE ONLY (Leave blank)		2. REPORT DATE	3. REPORT TYPE AND DATES COVERED FINAL/01 JUL 91 TO 30 JUN 93	
4. TITLE AND SUBTITLE STRUCTURE AND STABILITY OF REACTING COMPRESSIBLE FREE SHEAR LAYERS			5. FUNDING NUMBERS	
6. AUTHOR(S) DR GROSCH			2304/CS AFOSR-91-0250 61102F	
7. PERFORMING ORGANIZATION NAME(S) AND ADDRESS(ES) OLD DOMINION UNIVERSITY 46TH STREET & COLLEY AVENUE NORFOLD VA, 23508			8. PERFORMING ORGANIZATION REPORT NUMBER AFOSR TR 94 0167 94 0206 AFOSR TR 94 0167	
9. SPONSORING / MONITORING AGENCY NAME(S) AND ADDRESS(ES) AFOSR/NM 110 DUNCAN AVE, SUTE B115 BOLLING AFB DC 20332-0001			10. SPONSORING / MONITORING AGENCY REPORT NUMBER AFOSR-91-0250	
11. SUPPLEMENTARY NOTES				
12a. DISTRIBUTION / AVAILABILITY STATEMENT APPROVED FOR PUBLIC RELEASE: DISTRIBUTION IS UNLIMITED			12b. DISTRIBUTION CODE	
13. ABSTRACT (Maximum 200 words) The contract is in support of research on the structure and stability of reacting compressible mixing layers. The research performed under this contract has resulted in our learning a great deal about the structure and stability of reacting compressible mixing layers.				
14. SUBJECT TERMS			15. NUMBER OF PAGES	
			16. PRICE CODE	
17. SECURITY CLASSIFICATION OF REPORT UNCLASSIFIED	18. SECURITY CLASSIFICATION OF THIS PAGE UNCLASSIFIED	19. SECURITY CLASSIFICATION OF ABSTRACT UNCLASSIFIED	20. LIMITATION OF ABSTRACT SAR(SAME AS REPORT)	

DEPARTMENT OF COMPUTER SCIENCE
COLLEGE OF SCIENCES
OLD DOMINION UNIVERSITY
NORFOLK, VIRGINIA 23529

**REACTING COMPRESSIBLE MIXING LAYERS:
STRUCTURE AND STABILITY**

By

Chester Grosch, Principal Investigator

Final Report
For the period October 31, 1993

Prepared for
Air Force Office of Scientific Research
Building 410/NM
Bolling AFB DC 20332

Under
Research Contract AFOSR-91-0250
Dr. Marc Q. Jacobs, Program Manager

Submitted by the
Old Dominion University Research Foundation
P.O. Box 6369
Norfolk, Virginia 23508-0369

Accession For	
NTIS CRA&I	<input checked="" type="checkbox"/>
DTIC TAB	<input type="checkbox"/>
Unannounced	<input type="checkbox"/>
Justification	
By	
Distribution /	
Availability Codes	
Dist	Avail and/or Special
A-1	

October 1993

REACTING COMPRESSIBLE MIXING LAYERS: STRUCTURE AND STABILITY

C.E. Grosch

Old Dominion University
Norfolk, Virginia 23529

ABSTRACT

Understanding the structure and the stability characteristics of a reacting compressible mixing layer is of fundamental importance. Also, this flow can be regarded as the simplest relevant model of the combustion process in the scramjet. The theory describing the structure and stability of this flow is reviewed. This includes the structure of the mean flow and the combustion model, both of which determine the stability characteristics. Among the subjects included in the review of the stability characteristics are: the eigenvalue spectrum, convective Mach number, growth rates, and the transition from convective to absolute instability. Comparisons to experimental and numerical simulation results are made where possible.

1. Introduction

Understanding the stability characteristics of reacting compressible free shear flows is of fundamental importance (Jackson, 1992) and may have possible usefulness in the development of the scramjet engine (Beach, 1992). As discussed by Drummond and Mukunda (1988), the scramjet combustor flow is complex but spatially developing and reacting compressible mixing layers of fuel and oxidizer provide the simplest relevant model. In modeling this flow it is assumed that initially the fuel and oxidizer (and any non-reactive components) are in two unmixed co-flowing streams. Mixing of the two gases takes place in the shear layer between the streams and combustion occurs when there is both sufficient fuel and oxidizer present at the same point. The residence time of the fuel and oxidizer in the combustion chamber can be very short; therefore, it is extremely important that a high mixing rate be achieved so that complete combustion is attained before the fuel is convected out of the engine. Mixing is enhanced when the basic flow is unstable. Therefore knowledge of the flow's stability characteristics may improve the understanding of the mixing process in the scramjet and is also of fundamental interest in its own right.

It has been realized for some time that the problem of a very short residence time is compounded by the experimental observations that the mixing rates of shear layers decrease as the Mach number increases from zero (e.g., Brown and Roshko, 1974; Chinzei, Masuya, Komuro, Murakami, and Kudou, 1986; Papamoschou and Roshko, 1986, 1988; and Clemens, 1992). Numerical simulations of non-reacting compressible mixing layers (e.g., Guirguis, 1988; Lele, 1989; and Sandham and Reynolds, 1990) as well as reacting compressible mixing layers (Drummond and Mukunda, 1988; Drummond, Carpenter, Riggins, and Adams, 1989 for example) have also shown the same effect. It can be surmised that the initial growth of the mixing layer, formed by two turbulent boundary layers coming off a splitter plate, is entirely governed by entrainment due to the turbulent flow already present in the boundary layers. The scale of this motion is

that of the turbulent boundary layers on the splitter plate. Further downstream inviscid Kelvin-Helmholtz instabilities, with scales much greater than that of the original boundary layer, appear. These instability waves lead to the large "rollers" observed at low Mach numbers. These, in turn, entrain fluid, pair, and evolve toward the large scale structures which are observed further downstream. Observation and simulations suggest that, while the initial entrainment continues, the long wavelength Kelvin-Helmholtz instability is suppressed at higher Mach numbers. Because of this increased stability, natural transition to turbulence may be delayed and occur at downstream distances which are larger than practical combustor lengths resulting in incomplete combustion.

The dynamical processes governing reacting compressible flows are very complex, involving strong interaction between the chemical and fluid dynamical effects. Apart from a full numerical simulation of the chemistry and compressible fluid dynamics, including possibly turbulence modeling or large eddy simulation, any investigation of these flows must involve considerable modeling. This will, of necessity, rely heavily on the success achieved in modeling compressible non-reacting shear flows.

There is a very extensive literature dealing with stability and related topics for incompressible mixing layers (see Ho and Huerre (1984) for a comprehensive review) but, until quite recently, comparatively little dealing with even the non-reacting compressible flow. Earlier work on this problem has been reviewed by Jackson and Grosch (1989) as part of a comprehensive study of the stability of the non-reacting two dimensional compressible mixing layer. This study was extended to include the effect of variation in the thermodynamic properties on the stability characteristics (Jackson and Grosch, 1991) as well as the effect of three dimensionality of the mean flow due to skewing of the fast and slow streams (Grosch and Jackson, 1991a).

The structure and stability of the reacting flow is, of course, determined in part by the dynamics of the underlying non-reacting flow, in part by the reaction dynamics, and in part by the interaction of these two. In order to understand the dynamics of the reacting flow it is necessary to understand those of the non-reacting flow. Therefore in each section the results for the reacting flow are compared to those of the non-reacting flow.

In section 2 the structure of the mean flow is discussed. Section 3 contains a review of what is known of the stability of the compressible reacting mixing layer including, formulation of the problem (Section 3.1), the spectrum of the neutral waves (Section 3.2), the growth rates of unstable modes (Section 3.3), the convective Mach number (Section 3.4), and convective/absolute instabilities (Section 3.5). Finally, Section 4 contains concluding remarks.

2. Mean Flow: Ignition and Structure

A schematic of a reacting compressible mixing layer formed behind a splitter plate is shown in Figure 1. This shows the three regimes of ignition, deflagration, and diffusion flame (Linan and Crespo, 1976) which are expected to exist in this flow. The ignition regime is a region where the combustible gases mix until, at some finite distance downstream of the plate, a thermal explosion occurs and the gas is ignited. The second regime is the deflagration region. After ignition, a pair of well-defined deflagration waves (or "premixed flamelets") emerge according to classical thermal explosion theory. One of the flamelets is fuel-rich and the other is fuel-lean. There is excess fuel behind the fuel-rich flamelet and excess oxidizer behind the fuel-lean flamelet. Concentration

gradients behind the flamelets drive the unburnt fuel and oxidizer towards the diffusion flame where they are consumed. These waves penetrate the mixing layer until all of the deficient reactant is consumed. Just downstream of the deflagration wave, a diffusion flame regime exists where the mixing process is governed by diffusion in the direction normal to the flame.

Theoretical analysis of the ignition and structure of the reacting compressible mixing layer has been confined to steady two dimensional flows with a zero pressure gradient. Further assuming that the Reynolds number is large but that the flow can be modeled by a laminar flow, the basic equations are the equation of state for a perfect gas, the compressible boundary layer equations with a heat source term in the energy equation modeling the reaction, and the species mass fraction conservation equations.

$$1 = \rho T, \quad (1)$$

$$(\rho U)_x + (\rho V)_y = 0, \quad (2)$$

$$\rho(UU_x + VU_y) = (\mu U_y)_y, \quad (3)$$

$$\rho(UT_x + VT_y) = Pr^{-1}(\mu T_y)_y + (\gamma - 1)M^2\mu U_y^2 + \beta \Omega, \quad (4)$$

$$\rho(UF_{j,x} + VF_{j,y}) = Sc_j^{-1}(\mu F_{j,y})_y - \Omega_j. \quad (5)$$

These equations are nondimensionalized by the freestream values $T(\infty)$, $\rho(\infty)$, $U(\infty)$, $F_1(\infty)$ for the temperature, density, velocities and mass fractions, respectively, with lengths referred to some characteristic length scale of the flow. The x axis is along the direction of flow; the y axis is normal to the flow; U and V are the velocity components in the x and y directions, respectively; ρ is the density; T is the temperature; and $\{F_j\}$ are the mass fractions. The viscosity μ is assumed to be a function of temperature. The nondimensional parameters are the Prandtl number Pr , the Schmidt number $Sc_j = Pr Le_j$ for species j where Le_j is the Lewis number for species j, the Mach number $M = U(\infty)/a(\infty)$, with $a(\infty)$ the sound speed at $+\infty$, γ the specific-heats ratio, and β the heat release per unit mass fraction of the reactant. Finally, Ω is the reaction source term and $\{\Omega_j\}$ the species consumption rates. In the calculations of the mean flow and the stability calculations various models for the thermodynamic properties of the mean flow were used: (a) the Tanh model - the hyperbolic tangent profile for the mean speed and the Crocco relation for the mean temperature, with the Chapman viscosity-temperature relation and a Prandtl number of one; (b) the Lock model - the Lock profile for the mean speed and the Crocco relation for the mean temperature, with the Chapman viscosity-temperature relation and a Prandtl number of one; and (c) the Sutherland model - the similarity solution for the coupled velocity and temperature equations using the Sutherland viscosity temperature relation and arbitrary but constant Prandtl number.

A key element in the calculation is the specification of the combustion model, ie the form of Ω . Grosch and Jackson (1991b) assumed a one step irreversible reaction of the Arrhenius type between the fuel, F , (with mass fraction F_1) and the oxidizer, O , (with mass fraction F_2).



Taking

$$\Omega = D \rho F_1 F_2 e^{-Z_e/T}. \quad (7)$$

and

$$\Omega_1 = \Omega_2 = \Omega \quad (8)$$

with D the Damkohler number and the Zeldovich number $Ze = E/RT_\infty$ where E is the dimensional activation energy and R the universal gas constant. It is believed that this model will yield correct qualitative results but that there can be quantitative differences with the results of calculations using more accurate rate equation models. In any compressible flow calculations it is also necessary to specify the property variations with temperature and pressure. Because these authors used a simplified combustion model they also chose to use simple property variations: the Prandtl number constant and equal to one and a linear variation of the viscosity coefficient with temperature.

An appropriate set of initial (in x) and boundary (in y) conditions for the flow configuration of Figure 1 consistent with these equations is:

$$T = U = F_1 = 1, \quad F_2 = 0, \quad (9)$$

for $x = 0$, $y > 0$, and $x > 0$, $y \rightarrow \infty$.

$$T = \beta_T, \quad U = \beta_U < 1, \quad F_1 = 0, \quad F_2 = \frac{F_2(-\infty)}{F_1(\infty)} \equiv \phi^{-1}, \quad (10)$$

for $x = 0$, $y < 0$ and $x > 0$, $y \rightarrow -\infty$. Here ϕ is the equivalence ratio. If $\phi = 1$, the mixture is stoichiometric, if $\phi > 1$ it is fuel rich, and if $\phi < 1$ it is fuel lean. If β_T is less than one, the gas in the slow stream is relatively cold compared to that in the fast stream, and if β_T is greater than one it is relatively hot.

Grosch and Jackson (1991b) solved these equations by (1) numerically marching downstream in x (note that the equations are parabolic in x) and (2) by using a combination of large activation energy asymptotics and numerics to analyze the ignition and diffusion flame regimes. The numerical solution of these equations was facilitated by first transforming them into the incompressible form by means of the Howarth-Dorodnitsyn transformation

$$Y = \int_0^y \rho \, dy, \quad \hat{V} = \rho V + U \int_0^y \rho_x \, dy. \quad (11)$$

Solutions to the transformed equations were found by marching in x subject to the initial and boundary conditions (9 and 10) and it was found that the velocity profile, U , attained a self-similar form at a small value of x (Drummond and Mukunda, (1988) found that the solution of the Navier-Stokes equations also became self similar at small x). Because the solutions were self-similar, the independent variable Y was transformed to the similarity variable for the chemically frozen heat conduction problem

$$\eta = \frac{Y}{2\sqrt{x}}, \quad (12)$$

and all of the numerical calculations were carried out in the (x, η) variables.

The asymptotic analysis in the ignition regime was complicated by the necessity to consider a number of different cases depending on the magnitude of the dimensionless speed, β_U , and temperature, β_T , of the slow stream, and the Mach number, M . The cases analyzed were: (a) $|1 - \beta_T| \ll 1$, $|1 - \beta_U| \ll 1$, and $M = O(1)$, which is the case of ignition with nearly equal free stream temperatures and speeds (previously studied by Jackson and Hussaini (1988)); (b) $|1 - \beta_T| \ll 1$, $\beta_U < 1$, and $M \ll 1$, corresponding to

ignition in a shear flow at nearly equal free stream temperatures at small Mach number; and (c) $\beta_T > 0$, $0 \leq \beta_U < 1$, and $M > 0$.

The results are presented and compared in Figures 2 to 7. Figure 2 is a plot of the maximum temperature in the shear layer as a function of the downstream position at $M = 0$ and $M = 2$ for various values of Zeldovich number (Grosch and Jackson, 1991b). At $x = 0$ the temperature is that of the inert solution and for large x the temperature is that of the diffusion flame. It is clear that for the smaller value of the Zeldovich number ($Ze = 10$) a well defined ignition point does not occur; instead at both $M = 0$ and $M = 2$ there is a smooth and gradual transition from the inert solution at $x = 0$ to a diffusion flame. At the larger values of Ze there is a rapid transition from the inert solution to the diffusion flame solution, with the curves steepening as the Zeldovich number is increased. As the Zeldovich number increases, the solution approaches the infinite Zeldovich solution (dashed line) obtained from the asymptotic analysis for the ignition point and the diffusion flame. From this figure it is apparent that the ignition regime also exists in supersonic flows. As the Mach number increases there is a corresponding increase in the inert temperature at $x = 0$ due to viscous heating, thus lessening the relative effect of combustion on the overall temperature field. Also note that ignition occurs at a smaller value of x for the Mach 2 case as compared to that at zero Mach number.

Figures 3 and 4 show the corresponding temperature and mass fraction profiles as a function of position in the shear layer at various x locations for Mach numbers of 0 and 2, respectively. The rapid rise in the temperature (Figures 3a and 4a) over a narrow range of x indicates ignition. The temperature peak shifts and the profile is asymmetric due to the asymmetry in the velocity profile. The mass fraction profiles show that there is a diffusion of F_1 from the $\eta \geq 0$ region into the $\eta \leq 0$ region with $F_1 = 0$ only at $\eta = -\infty$. At larger x there is a small secondary maximum in the F_1 distribution in $-3 < \eta < -1$ showing the presence of a premixed flamelet in this region. As first pointed out by Linan and Crespo (1976), these arise because the mixture is not stoichiometric in the premixed region. One of the reactants is consumed locally, leaving behind an excess of the other reactant. These premixed flamelets are quite weak in that the temperature rise associated with them is small. The distribution of F_2 is the converse of that of F_1 .

The existence of the premixed flamelets and the diffusion flame is shown quite clearly in Figure 5a, which shows the loci in the (x, η) plane of the maxima of Ω (the chemical production term) for equal free stream temperatures ($\beta_T = 1.0$). The adiabatic diffusion flame temperature is 1.5 and is greater than the free stream temperature. As shown in this figure, the position of the maximum decreases from about $\eta = -0.2$ at $x = 0$ to nearly $\eta = -0.6$ at $x \approx 2.9$. The maximum value of Ω increases along this curve. At $x \approx 2.9$ ignition occurs and two maxima appear giving rise to the premixed flamelets. Beyond the ignition point the premixed flamelets move outwards in the shear layer until all of the deficient reactant is consumed. The appearance of the third maxima just behind the ignition point marks the appearance of the diffusion flame. As x is further increased, the diffusion flame becomes dominant and, as $x \rightarrow \infty$, the diffusion flame thins and approaches a flame sheet characterized by local chemical equilibrium and described by the asymptotics. Figure 5b shows similar results for the same values of the parameters except that $\beta_T = 0.5$ and $\beta = 1.5$. This case corresponds to unequal freestream temperatures. The adiabatic flame temperature is again 1.5 and is larger than either freestream temperature. The ignition point has moved into the region of

higher freestream temperature and the location of the diffusion flame is unchanged while that of the premixed flamelets has changed. Figure 5c shows results for $\beta_T = 0.5$ and $\beta = 0.4$. The adiabatic flame temperature in this case is 0.95 and is smaller than the freestream temperature at $+\infty$. In contrast to the two previous figures, there is no well defined ignition point; the premixed flame merges smoothly into the diffusion flame whose location is unchanged. In addition, the premixed flamelets are absent. Finally, it should be noted that the authors stated that the behaviour shown in Figure 5 also was found for Mach numbers greater than zero. Detailed predictions of location of the ignition point as a function of the flow parameters were also made via the large Ze asymptotic analysis. The results showed that the ignition point moves toward the origin as the Mach number is increased, in agreement with the numerical results.

From both the numerical and asymptotic results it is apparent that the ignition regime exists in supersonic as well as subsonic and incompressible flows. As the Mach number increases there is a corresponding increase in the inert temperature at $x = 0$ due to viscous heating, thus lessening the relative effect of combustion on the overall temperature field. Also note that ignition occurs at a smaller value of x for the Mach 2 case as compared to that at zero Mach number.

The diffusion flame regime was analyzed by considering the limit of infinite Damkohler number. Grosch and Jackson showed that solutions for the mean flow could be found in terms of certain integrals of the velocity profile. In the case of $Pr = Le = 1$ this solution reduced to the flame sheet solution (Jackson and Grosch, 1990b). When these parameters are not unity it was necessary to evaluate the results numerically. The location of the flame sheet as a function of Sc_1 for various values of β_U , the slow stream nondimensional speed, ϕ , the equivalence ratio, and Sc_2 is shown in Figure 6. As Sc_2 or ϕ is increased the flame sheet moves into the slower moving stream, but as β_U is increased it moves into the faster stream.

3. Stability of the Reacting Compressible Mixing Layer

Rapidly growing broadband instabilities will generally enhance mixing and thus promote rapid and complete combustion. The current state of knowledge of the stability of the reacting compressible mixing layer is reviewed here. The topics reviewed include: the spectrum of the neutral modes, the growth rates of the unstable modes, and the convective Mach number. Finally, the recent results on the transition from convective to absolute instability in this flow is reviewed.

3.1 Formulation of the Stability Problem

It is generally agreed that the stability of free shear layers, both incompressible and compressible, is dominated by inviscid dynamics. Thus the governing equations for the stability problem are the compressible Euler equations. In the reacting case the source terms for the temperature and mass fractions must also be included if the combustion is modeled by finite rate chemistry. In the flame sheet limit the perturbation does not affect the heat release in the sheet, it merely wrinkles the sheet. Therefore, the only effect the reaction has on the flow stability is through the change in the mean temperature distribution from that of the non-reacting flow. With finite rate chemistry, the perturbations not only wrinkle the combustion zone but also change the rate of heat release in the reaction through changes in the temperature and mass fraction distribution

within the combustion zone. The change in heat release then effects the temperature and mass fraction distributions. This, in turn, affects the stability of the flow.

To date there have been very few studies of this problem (Jackson and Grosch, 1990b; Hu, Jackson, Lasseigne and Grosch, 1993; Shin and Ferziger, 1990 and 1991; and Planche and Reynolds, 1991). The starting point for all of these studies is the compressible Euler equations with the source terms those for a one step irreversible reaction of the Arrhenius type (equations (6) - (8)). All of the published studies make the parallel flow assumption in the derivation of the stability equations. However, it is straightforward to apply a weakly nonparallel approach to this stability problem. In this approach one obtains the parallel flow equations as the first approximation and also finds the next order correction to the growth rate.

The equation for the amplitude of the pressure perturbation is

$$\begin{aligned} \Pi'' - [2U'/(U - c) + (1 - K_1) T'/T] \Pi' \\ - \alpha^2 T [T - K_2 M^2 \cos^2 \theta (U - c)^2] \Pi = 0, \end{aligned} \quad (13)$$

where

$$K_1 = J_3/J_1, \quad (14)$$

$$K_2 = \gamma - (\gamma - 1)(J_2/J_1), \quad (15)$$

and

$$J_1 = 1 + i \frac{(\beta Q_3 - Q_1 - Q_2)T}{\alpha \cos \theta (U - c)}, \quad (16)$$

$$J_2 = 1 - i \frac{(Q_1 + Q_2)T}{\alpha \cos \theta (U - c)}, \quad (17)$$

$$J_3 = 1 - i \frac{(Q_1 H_1' + Q_2 H_2')T}{\alpha \cos \theta T' (U - c)}, \quad (18)$$

$$Q_1 = \frac{\partial \Omega}{\partial F_1}, \quad Q_2 = \frac{\partial \Omega}{\partial F_2}, \quad Q_3 = \frac{\partial \Omega}{\partial T}, \quad (19)$$

and

$$H_j = T + \beta F_j, \quad (20)$$

with the primes indicating differentiation with respect to the similarity variable η . Here α is the wavenumber, θ is the direction of propagation of the disturbance wave in the $(x - z)$ plane, $c = \omega/\alpha$ is the complex phase speed and ω is the frequency. For spatial theory, ω is required to be real and solutions are sought for which α is complex. For temporal theory, α is assumed to be real and solutions are sought for which ω is complex. The amplification rates of the disturbances are then $-\alpha_i$ or ω_i , respectively. The disturbances are two dimensional for $\theta = 0^\circ$ and otherwise oblique.

If $\beta = 0$ it is easily seen that $K_1 = K_2 = 1$ and equation (13) reduces to the compressible Rayleigh equation governing the stability of the non-reacting flow (Jackson and Grosch, 1989). If a flame sheet model is used instead of a finite rate chemistry model the reaction is confined to a sheet of zero thickness and $\beta = 0$ outside of the sheet. Thus the stability equation is again (13) with $K_1 = K_2 = 1$ and, of course, the appropriate velocity and temperature distributions for the flame sheet model (Jackson and Grosch, 1990b; Hu, Jackson, Lasseigne, and Grosch, 1993).

The boundary conditions for Π are obtained by considering the limiting form of (13) as $\eta \rightarrow \pm\infty$ which gives

$$\Pi \rightarrow e^{(\pm \Delta_{\pm} \eta)}, \quad (21)$$

where

$$\Delta_+^2 = \alpha^2 [1 - M^2 \cos^2 \theta (1 - c)^2], \quad (22)$$

$$\Delta_-^2 = \alpha^2 \beta_T [\beta_T - M^2 \cos^2 \theta (\beta_U - c)^2]. \quad (23)$$

The values of the phase speed for which Δ_{\pm}^2 vanishes are

$$c_+ = 1 - \frac{1}{M \cos \theta}, \quad (24)$$

$$c_- = \beta_U + \frac{\sqrt{\beta_T}}{M \cos \theta}, \quad (25)$$

where c_+ is the phase speed of a sonic disturbance in the fast stream and c_- is the phase speed of a sonic disturbance in the slow stream. For

$$M \cos \theta = M_* = \frac{1 + \sqrt{\beta_T}}{1 - \beta_U} \quad (26)$$

c_{\pm} are equal.

The nature of the disturbances for the stability problem can be illustrated by Figure 7 (Jackson and Grosch, 1989), which is a plot of c_{\pm} versus M for $\beta_T = 0.5$, $\beta_U = 0$, and $\theta = 0^\circ$. These curves divide the phase speed-Mach number plane into four regions. If a neutral disturbance exists with a Mach number and phase speed in region 1, it is subsonic at both boundaries, and is classified as a subsonic neutral mode. In region 3, the neutral disturbance is supersonic at both boundaries, and is classified as a supersonic-supersonic neutral mode. In region 2, the neutral disturbance is subsonic in the fast stream and supersonic in the slow stream, and is classified as a fast neutral mode. Finally, in region 4, the neutral disturbance is supersonic in the fast stream and subsonic in the slow stream, and is classified as a slow neutral mode. For oblique modes ($\theta \neq 0^\circ$) the four regions still exist and only the boundaries, as defined by the c_{\pm} curves in the phase speed - Mach number plane, are changed from those of the two dimensional modes (Grosch and Jackson, 1991a). Finally, it is important to note that the sonic speeds are independent of the reaction since the far field is chemically frozen. Thus the classification scheme does not depend on the reaction model used.

Because of causality there can be no incoming waves for an unbounded domain, unless the flow is being driven by an external source. Assuming that this is not the case, boundary conditions for an unbounded domain require that the far field solution be outgoing waves. The appropriate boundary condition for outgoing waves in the fast stream is,

$$\Pi \rightarrow e^{(-\Delta_+ \eta)}, \quad (27)$$

if $c_r > c_+$, and

$$\Pi \rightarrow e^{(-i \eta \sqrt{-\Delta_+^2})}, \quad (28)$$

if $c_r < c_+$. For the slow stream the appropriate boundary condition for outgoing waves is,

$$\Pi \rightarrow e^{(\Delta - \eta)}, \quad (29)$$

if $c_r < c_-$, and

$$\Pi \rightarrow e^{(-i\eta \sqrt{-\Delta_-^2})}, \quad (30)$$

if $c_r > c_-$.

For a bounded domain the boundary condition is that the pressure gradient normal to the boundary is zero. Thus, on the boundaries

$$\hat{n} \cdot \nabla \Pi = 0, \quad (31)$$

with \hat{n} the unit normal to the boundary.

3.2 The Spectrum of Neutral Waves

Both the non-reacting and reacting mixing layers have a complicated eigenvalue spectrum. The first step in finding and analyzing this spectrum is to find the neutral modes. For the subsonic modes, which lie in region 1 of the $c_r - M$ diagram, a theorem of Lees and Lin (1946) can be used. This result is derived from consideration of the equation governing the normal velocity perturbation \hat{v} . The disturbance equation for the normal velocity component is (Jackson, 1992)

$$(\xi e^H \hat{v}')' - e^H (q + \alpha^2) \hat{v} = 0, \quad (32)$$

where

$$\xi = T^{-1} (T - K_2 M^2 (U - c)^2)^{-1}, \quad (33)$$

$$H = - \int (1 - K_1) (T'/T) d\eta, \quad (34)$$

and

$$q = [\xi (U' + (U - c) (1 - K_1) (T'/T))]' / (U - c). \quad (35)$$

Note that (32) has a singularity at $U = c$. Define

$$S(\eta) \equiv \frac{d}{d\eta} (T^{-2} \frac{dU}{d\eta}). \quad (36)$$

Let $\tilde{c} = U(\eta_c)$, where η_c is a root of $S(\eta)$. If \tilde{c} lies in region 1 of the $c_r - M$ diagram (Figure 7), then (Lees and Lin, 1946) $\tilde{c} \equiv c_N$ is the phase speed of a neutral mode provided that $\alpha \neq 0$. The corresponding neutral wave number and frequency must be determined numerically. These modes are the regular subsonic neutral modes.

In addition to the neutral modes with $\alpha_N \neq 0$ there may exist neutral modes having zero wavenumber. The phase speed of such modes do not satisfy (36) but can be found by an asymptotic analysis of (13) in the limit $\alpha \rightarrow 0$ (Hu, Jackson, Lasseigne, and Grosch, 1993). The result of this analysis is, for $M = \beta_U = 0$,

$$c_N = \frac{1 + i e^{B/2}}{1 + e^B}, \quad (37)$$

with

$$B = \int_{-\infty}^{\infty} \frac{(F_1 + F_2)T' + \beta(F_1 F_2)'}{(F_1 + F_2)T - \beta(Ze - 1)F_1 F_2 T'} d\eta. \quad (38)$$

In the nonreactive case ($\beta = 0$) this reduces to

$$c_N = \frac{\beta_T + i\sqrt{\beta_T}}{\beta_T + 1}, \quad (39)$$

which shows that the neutral phase speed is complex for $\alpha_N = 0$.

If \bar{c} lies in regions 2, 3, or 4 of the $c_r - M$ diagram, then \bar{c} does *not* correspond to the phase speed of a true neutral mode. The phase speed of the neutral modes in these regions must, in general, be found numerically. One exception is the supersonic-supersonic neutral modes with $\alpha = 0$ (Grosch, Jackson, Klein, Majda, and Papageorgiou, 1991). In this case an expansion of the solution in powers of α , along the lines previously used by Drazin and Howard (1962) and Blumen, Drazin and Billings (1975) in related studies, yields an eigenvalue relation which is analytically tractable.

The leading-order term in the expansion is independent of the detailed form of U and T , and only depends on the basic flow characteristics at infinity. This is to be expected from physical arguments because the wavelength of the instability in the limit $\alpha \rightarrow 0$ is much larger than the length scale over which the undisturbed flow is non-uniform. Setting the leading-order term in the expansion to zero yields an equation for $c \equiv c_N$:

$$\beta_T [M^2(\beta_U - c_N)^2 - \beta_T](1 - c_N)^4 = [M^2(1 - c_N)^2 - 1](\beta_U - c_N)^4. \quad (40)$$

This equation is identical to (5.3a) of Miles (1958) if his result is expressed in the notation used here. Miles showed (in this notation) that:

[1] A single real root of (40) exists for

$$M \geq M_* \equiv (1 + \sqrt{\beta_T})/(1 - \beta_U), \quad (41)$$

with phase speed

$$c_N = (\beta_U + \sqrt{\beta_T})/(1 + \sqrt{\beta_T}). \quad (42)$$

This is classified as a constant speed supersonic-supersonic neutral mode lying in region 3 of the $c_r - M$ plane. It is independent of Mach number and corresponds to the phase speed at which the sonic speeds in the two streams are equal. In this regime there is also a pair of complex conjugate eigenvalues corresponding to one unstable and one stable eigenmode. The associated instability is analogous to the classical Kelvin-Helmholtz instability for subsonic vortex sheets (Artola and Majda, 1987). This instability disappears as the Mach number increases.

[2] A double root first appears at

$$M_{CR} = (1 + \beta_T^{1/3})^{3/2}/(1 - \beta_U), \quad (43)$$

with phase speed

$$c_N = (\beta_U + \beta_T^{1/3})/(1 + \beta_T^{1/3}). \quad (44)$$

There are three distinct real roots for $M > M_{CR}$. One of these is the phase speed of the constant speed supersonic-supersonic neutral mode while the other two roots must be found numerically from (40). For the special case of $\beta_T = 1$, these roots are given by

$$c_N = \frac{1 + \beta_U}{2} \pm \frac{1}{2M} [M^2(1 - \beta_U)^2 + 4 - 4(M^2(1 - \beta_U)^2 + 1)^{1/2}]^{1/2}. \quad (45)$$

The root which corresponds to the (+/-) sign is classified as a fast/slow supersonic-supersonic neutral mode. Note that all three of these neutral modes lie in region 3.

The neutral phase speeds given above are exact for $\alpha = 0$. In order to obtain the higher order corrections for $\alpha \neq 0$ the value of c must also be expanded in powers of α . When this was done it was found that the overall growth rate was $O(\alpha^2)$. (Balsa and Goldstein (1990) also found, numerically, the $O(\alpha^2)$ growth rate for these modes.) It was also found that the growth rate at $O(\alpha^2)$ becomes singular at M_{CR} . This singular behaviour was studied by expansions about the singular value of M . A connection between the regimes $M_* < M < M_{CR}$ and $M > M_{CR}$ was found and yielded the transition from a stable/unstable pair of eigenmodes plus a supersonic neutral mode for $M < M_{CR}$ to three supersonic neutral modes for $M > M_{CR}$.

The asymptotic expansion for the supersonic-supersonic modes gave the neutral curves in region 3. The other regions of the $c_r - M$ diagram were also investigated numerically using all three of the thermodynamic models (Grosch, et al, 1991). Representative results are presented in Figure 8 for the case of the Tanh and Sutherland profiles. Note the qualitatively similar results of these models. Plots of the phase speed c_N of the neutral modes as a function of the Mach number are shown in this figure.

In order to understand the variation of phase speed of the neutral modes with β_T and M it is important to recall (Jackson and Grosch, 1991) that, for each thermodynamic model, there exists a transition value of β_T , denoted by $\hat{\beta}_T$. For $\beta_T = \hat{\beta}_T$, the neutral mode phase speed is independent of M in region 1. For $\beta_T > (<) \hat{\beta}_T$, c_N is a monotonically increasing (decreasing) function of M in region 1. The value of $\hat{\beta}_T$ is 1.0, 0.57753, and 0.445 for the Tanh, Lock, and Sutherland ($Pr = 1$) profiles, respectively. For all β_T there are two subsonic neutral modes, labeled in this figure by 1 and 2. Mode 1 is that whose phase speed is found from the regularity condition (equation (36), above) and mode 2 is found numerically as $(\alpha, \omega) \rightarrow 0$ with $c \neq 0$. Because of the symmetry of the Tanh velocity and temperature profiles, the phase speeds of these two modes are identical at $M = 0$ for any β_T and also for all Mach numbers in region 1 when $\beta_T = 1$. In Figure 8a, $\beta_T = 2$ and is greater than the transition value for both models. Thus as the Mach number is increased, mode 1 is transformed into a fast supersonic mode (labeled 3 in Figure 8a) and mode 2 is transformed into a supersonic-supersonic mode. Mode 4 is the slow supersonic mode which appears at $M = M_*$. Mode 5 is the constant speed supersonic-supersonic mode which also appears at $M = M_*$. Modes 6 and 7 are the fast and slow supersonic-supersonic modes which exist for $M > M_{CR}$. Note that, with $\beta > \hat{\beta}_T$, mode 2 merges with mode 7, the slow supersonic-supersonic mode, at an M near M_{CR} . The phase speed curves of Figure 8b show the symmetry due to the Tanh profiles when $\beta_T = \hat{\beta}_T = 1$. Modes 1 and 2 coincide in region 1 as do modes 2 and 5 for $M_* \leq M \leq M_{CR}$ in region 3. The phase speeds of modes 1 and 2 for the Sutherland model do not coincide in region 1. The results shown in Figure 8c are for $\beta_T = 0.5 < \hat{\beta}_T$ for the Tanh model but $> \hat{\beta}_T$ for the Sutherland model. Because of this, mode 1 merges, with increasing Mach number, with mode 4, the slow supersonic mode, at an M near M_{CR} for the Tanh model. However, for the Sutherland model, mode 1 still merges with mode 3, the fast supersonic mode as the Mach number increases.

Coalescence and switching of a pair of unstable modes was found by Grosch, et al (1992) at other values of the parameters and for the other thermodynamic models. This phenomena is not a feature solely due to the symmetry of the profiles of the Tanh model at $\beta_T = 1$. An example of coalescence and mode switching, with $\beta_T = 2$, is shown in Figure 9, for the Tanh model. This is a plot of ω_i versus ω_r (9a) and c_r versus c_i (9b) at

two Mach numbers which closely bracket the mode switch. At $M = 2.86$ (dashed curve) the fast supersonic mode has its neutral value on curve 2 of Figure 9 and its growth rate goes to zero linearly with α . The slow supersonic mode has its neutral point on curve 5, the constant speed supersonic-supersonic neutral mode. Its growth rate goes to zero quadratically with α . At $M = 2.88$ (solid curve) these two modes have switched. The switching is most clear in Figure 9b.

The addition of the reaction further increases the complexity of the spectrum of the disturbances. Consider first the flame sheet model. Because T' is discontinuous at the flame sheet for nonzero β , $S(\eta)$ will also be discontinuous at this point. It was found (Jackson and Grosch, 1990b) that S can have a single root, two roots one of which corresponds to η positive and the other negative, or two roots one of which is a one-sided zero. The roots of S , which corresponds to phase speeds that are subsonic at both boundaries, are the phase speeds of subsonic neutral modes. The one-sided zero of S may or may not yield a phase speed of a neutral mode. Finally, for non-zero β , there can also be singular neutral modes whose phase speeds are not given by roots of S and are subsonic at the boundaries. If the phase speed corresponding to a zero of S is supersonic at either or both boundaries it may or may not be that of a neutral mode. This can only be determined numerically.

In order to illustrate the complexity, results for a typical case obtained using the flame sheet model with a Tanh profile (Jackson and Grosch, 1990) are shown. The phase speeds of the neutral modes for $M = 0$ and $\beta_T = 2.0$ are plotted as a function of β with $\phi = 0.5, 1.0, 2.0$ in Figure 10. There are both fast and slow subsonic neutral modes. It was shown that, for the Tanh model with $M = 0$, fast waves only exist for

$$\beta \geq 1 - \beta_T \phi \quad (46)$$

with corresponding neutral phase speed

$$c_N = \frac{\beta + \beta_T \phi}{\beta + (1 + \beta_T) \phi}, \quad (47)$$

while slow waves only exist for

$$\beta \geq \beta_T \phi - 1 \quad (48)$$

with corresponding neutral phase speed

$$c_N = \frac{\beta_T}{1 + \beta + \beta_T}. \quad (49)$$

In addition, there are both fast and slow singular subsonic neutral modes, adjacent to their corresponding regular neutral modes. The phase speeds of these singular modes are independent of β . These modes are labeled FSP (Flame Sheet Primary) and FSS (Flame Sheet Secondary) in the figure. These singular modes have both zero wavenumber and frequency.

An important question is the extent to which this mode structure is an artifact of (a) the Tanh model and (b) the flame sheet model. At least a partial answer was provided by Hu, Jackson, Lasseigne, and Grosch (1993). They compared the phase speeds of the neutral modes at $M = 0$ using the finite rate model discussed in Section 2 and a flame sheet model, both with $P\tau = 1$ and a linear viscosity-temperature relation (the Lock model). The phase speed of the singular modes with zero wavenumber was found by using equations (38) or (39).

Figures 11a,b are plots of S versus η for various values of the heat release parameter, β , using the finite rate model. The slow stream has a speed $\beta_U = 0$ and temperature $\beta_T = 0.5$ and the equivalence ratio $\phi = 1$. The results shown in Figure 11a were obtained using the temperature distribution upstream of ignition while those of Figure 11b were obtained using the temperature distribution far downstream of ignition where the temperature and mass fraction concentrations are close to those of the flame sheet. The rate of heat release has a significant effect not only on the number of roots of S , but also on their values. When the heat release parameter is small ($\beta = 0.1$), there is a single root of S with η_c close to zero at both locations. With $\beta = 1.5$ there are three roots of S at the downstream location, one at $\eta \approx -0.5$ and a double root close to $\eta = 0$. A further increase in β to 2 results in a shift of the first root to more negative values of η and a splitting of the double root into two distinct roots, one close to zero and the other near $\eta = 1$. Qualitatively similar behavior is shown in Figure 11b at the downstream location.

The corresponding neutral phase speeds (indicated by boxes) obtained from the roots of S are shown in Figure 11c and 11d for the upstream and downstream locations, respectively, both for $\beta_T = 0.5$ and 11e and f, again upstream and downstream of ignition, with $\beta_T = 1$. These are shown as functions of the heat release parameter β . The real part of the neutral phase speeds for the $\alpha_N = 0$ mode, found from (38), are shown in these figures by inverted triangles. The flame sheet model results are shown as dashed lines in these figures.

In the nonreactive case ($\beta = 0$), there are two neutral modes with different phase speeds which coincide at $\beta_T = 0.57753$ (Jackson and Grosch, 1990b). With $\beta_T = 0.5$ these are slow neutral modes. One of these neutral modes has a phase speed determined by a root of S and the other member of this pair has a phase speed determined by (39). With $\beta_T = 1$, these neutral modes are fast modes since they have phase speeds greater than 0.5. Again, one of these has a phase speed determined by a root of S and the other member of this pair has a phase speed determined by (39).

When heat release is included ($\beta > 0$) and the flame sheet model is used (denoted by the dashed lines) there are, in general, four neutral modes: two are found from the Lees and Lin condition, called modes 1 and 2; one is found from the zero wavenumber asymptotics, called mode 3; and the remaining one, mode 4, is a mode with phase speed $c_N = U(\eta_f)$ where η_f is the location of the flame sheet. Mode 1 is a slow mode for $\beta_T < 0.57753$ and its phase speed is a decreasing function of β (Figures 11c,d); while for $\beta_T > 0.57753$, mode 1 is a fast mode whose phase speed is an increasing function of β (Figures 11e,f). Mode 2 only exists for $\beta > 0$ and shows the opposite behavior of mode 1. The third neutral mode, that with $\alpha_N = 0$, exists at $\beta = 0$ and has a phase speed which is constant for all values of the heat release parameter, β . Finally, the fourth neutral mode appears at the same value of β as the second mode, has a phase speed which is equal to $U(\eta_f)$ and is independent of β . When both streams have the same temperature, $\beta_T = 1$, the phase speeds of the third and fourth modes are equal. These neutral curves separate stable from unstable regions with an unstable region lying between modes 1 and 3 (called the slow branch) and another between modes 2 and 4 (called the fast branch).

As with the flame sheet model, there are also four neutral modes when using the finite rate chemistry model. The phase speeds of modes 1, 2 and 4 are determined from the Lees and Lin condition, and the third neutral mode is again the zero wavenumber mode with phase speed determined from (38). The reason the fourth mode of the

flame sheet model is not determined from (36) is that the Lees and Lin condition fails to hold because S is discontinuous and the derivatives of the eigenfunctions become discontinuous at the flame sheet position. For the finite rate chemistry model, the phase speed of the fourth neutral mode approaches that given by mode 4 of the flame sheet model, i.e., $c_N \rightarrow U(\eta_f)$, as x increases. The phase speeds of the neutral modes 1, 2, and 4 are indicated by boxes in Figures 11c-e, and the phase speed of the third neutral mode is indicated by inverted triangles. Unlike the flame sheet model, the neutral phase speeds for modes 3 and 4 are functions of the heat release parameter β and the downstream position x .

The value of the phase speeds of all four neutral modes will depend critically on whether the x location is upstream or downstream of ignition. In the region of ignition, the temperature and mass fraction fields vary rapidly with position and consequently the parallel flow approximation no longer holds. If x is sufficiently downstream of the ignition point, neutral modes 2 and 4 are present. At $x = 3$ and with $\beta_T = 0.5$ (Figure 11c) the phase speeds of neutral mode three show large variations between $0.5 < \beta < 2$. This is to be expected because ignition occurs in this region and the parallel flow assumption fails. As β is increased past 2, the phase speeds of all four neutral modes approach the phase speeds predicted by the flame sheet model. Similar behavior is shown in Figure 11d at $x = 10$. The variations in the real part of the phase speeds of the $\alpha_N = 0$ neutral mode appear smaller than at $x = 3$ which is consistent since the source term is proportional to $x\beta$ and thus at larger x the ignition region extends over a smaller range of β .

These results indicate that the flame sheet is a good approximation to the the flow and combustion field resulting from using finite rate chemistry to calculate the flame, as least as far as is required for stability analysis. However, the finite rate chemistry model used in these calculations is the one step irreversible model given by equations (6) - (8). It is also important to determine how sensitive the results of the stability calculations are to the details of finite rate chemistry model. It appears that almost nothing has been done to address this problem.

The only results currently available are those of Hu (1992). He used the Birkan and Law (1988) three step chain reaction model



where F , O , P and M are the fuel, oxidizer, product, an inert third body and R_1 and R_2 are radicals. The first two reactions are irreversible, thermoneutral, high activation energy branching reactions. The third reaction is a highly exothermic, zero activation energy, three body termination reaction. Hu repeated the calculations of Grosch and Jackson (1991b) for the mean velocity, temperature, and mass fraction distributions with the Birkan-Law reaction replacing the one step irreversible reaction (equation (6)).

This required having four equations for the mass fraction distributions, $\{F_j\}$ $j = 1, 2, 3, 4$, one each for F , O , R_1 and R_2 , respectively. The reaction rates, w_j , for equations (50) - (52) were modeled by

$$w_1 = D_1 F_1 F_3 e^{Zc(1-1/T)}, \quad (53)$$

$$w_2 = D_2 F_2 F_4 e^{2\epsilon(1-1/T)}, \quad (54)$$

$$w_3 = D_3 F_3 F_4. \quad (55)$$

Then in equations (4) and (5)

$$\Omega = w_3, \quad (56)$$

$$\Omega_1 = -w_1, \quad (57)$$

$$\Omega_2 = -w_2, \quad (58)$$

$$\Omega_3 = -w_1 + 2w_2 - w_3, \quad (59)$$

and

$$\Omega_4 = 2w_1 - w_2 - w_3. \quad (60)$$

Hu then used the calculated velocity and temperature distributions to calculate $S(\eta)$ (equation (36)) in order to find its roots and thus the phase speeds of the subsonic neutral modes as a function of β . His results for $M = 0$, $\beta_U = 0$ and $\beta_T = 0.5$ are shown in Figure 12, with 12a being a plot of $S(\eta)$ for selected values of β and 12b being a plot of the phase speeds of the neutral modes c_N as a function of β . These results should be compared to those of Figures 11b and 11f which are the equivalent results for the same values of the parameters using the one step irreversible reaction. The general behavior of the $S(\eta)$ curves in Figure 12a is similar to that of Figure 11b. The agreement between the c_N s of 11f and 12b is extremely good. On the basis of this very limited evidence, it appears that the spectrum of the neutral modes may not be very sensitive to the details of the chemistry model.

Figure 13 is a plot of the c_N as a function of the Mach number for $\beta_T = 2$, $\phi = 1$ and various values of $\beta > 0$ using the flame sheet model. The structure of the neutral mode spectrum at $M = 0$ is here extended into the range of non-zero Mach numbers. There is an increase in the phase speed of the fast modes as β is increased. The phase speed of the slow supersonic modes of region 4 decreases with increasing β and, for $\beta > 1$, a singular subsonic neutral mode with $c_N = 0.5$ appears in region 1. Correspondingly, for $\beta > 0$, there also exists a singular subsonic neutral mode in region 1 associated with the fast modes. Again the curves for the fast and slow neutral modes are each asymptotic to a single curve for large M . As in other cases, an increase in β causes an increase in the range of the phase speeds of the unstable waves and hence an increase in the dispersion. Jackson and Grosch (1990b) also reported calculations of c_N as a function of the Mach number with fixed β_T and β for various values of ϕ . It was reported that, as the equivalence ratio ϕ increased, the phase speed of the slow mode was unchanged, consistent with the Mach zero results (see equation (39)). The only effect was a change in the critical value of the Mach number below which this neutral mode did not exist; the smaller the value of ϕ the larger was the value of the critical Mach number. The phase speed of the fast neutral modes was reported to decrease with increasing ϕ . Finally, it should be noted in Figure 13 that, at larger Mach numbers, the neutral modes have quite different phase speeds. Consequently the associated unstable waves will also have much different phase speeds. They will appear as fast and slow unstable waves.

3.3 Growth Rates

The spectrum of the neutral modes has been found to be rather complex and that of the unstable modes is, of course, equally complex. Perhaps the most striking feature

is the existence, at supersonic Mach numbers, of two bands of unstable modes; the fast and slow unstable modes. For the non-reacting flow it has been shown (Jackson and Grosch, 1991) that the growth rates are not very sensitive to the detailed shape of the mean velocity and temperature profiles. This is shown by the results presented in Figures 14 and 15.

These figures show the variation of the growth rate with the frequency of the disturbance, for both the fast and slow unstable supersonic modes with $\beta_T = 2.0$ and $M = 2.5$ and $M = 5.0$ for the three thermodynamic models: Tanh, Lock and Sutherland. In both cases the slow unstable supersonic modes exist in a very narrow range of frequencies compared to that of the unstable fast supersonic modes. The shape of the $-\alpha_i$ versus ω curves is similar for all of the models with the maximum growth rate of the fast modes being substantially greater than that of the slow modes. This is a result of β_T of 2.0 being greater than the critical value, $\hat{\beta}_T$, as discussed in Section 3.2. The double maximum in the growth rate curves for the fast modes at $M = 2.5$ is quite characteristic. It occurs because there is a mode switch, as discussed in the previous Section, at an near value of β_T .

Figure 16 shows the maximum growth rates versus Mach number with $\beta_T = 2.0$, again for the non-reacting flow. The general variation is similar for all of the thermodynamic models. The maximum growth rate is largest at Mach zero and decreases by a factor of 5 to 10 as the Mach number increases from zero to M_* and approaches a limiting value as the Mach number is further increased. The second group of unstable modes, the slow supersonic modes, appear just below M_* . The growth rate of the most unstable of these modes first increases over a small range of Mach numbers and then decreases, approaching a limiting value at larger values of the Mach number. These results are typical of those found at other values of β_T (Jackson and Grosch, 1990b).

The effect on the stability of the non-reacting compressible mixing layer of a skewing of the streams at $\pm\infty$ has also been investigated (Grosch and Jackson, 1991a). The mean flow at $+\infty$ has a magnitude of 1.0 and is at an angle ψ with respect to that at $-\infty$, which has a magnitude β_U . These parameters can be restricted to $0^\circ \leq \psi \leq 90^\circ$ and $0 < \beta_U \leq \cos \psi$. The direction of propagation of the disturbance, θ , was also taken to be non-zero.

The theorems of Rayleigh and Howard provide bounds on the phase speed and/or growth rates of temporally growing disturbances in unstable, inviscid, incompressible shear flows (see Drazin and Reid (1984) for a comprehensive review). Some of these results have been extended by Chimonas (1970) so as to include compressibility. Similar results were also obtained by Djordjevic and Redekopp (1988). Chimonas' results were further extended by Grosch and Jackson to include crossflow, with the extension applying to flows in a channel with boundaries at a finite distance or in an infinite domain provided the disturbances are subsonic, and hence decay, at $\pm\infty$. The Lees and Lin condition for the existence of a regular subsonic neutral mode was extended to the case of crossflow. The definition of the convective Mach number (Jackson and Grosch, 1990a) was also generalized. Finally it was shown that, at zero Mach number, a generalization of Squire's theorem could be found.

Results of calculations of the growth rates showed that a non-zero crossflow ($\psi > 0$) combined with an obliquely propagating disturbance ($\theta > 0$) could have an appreciable effect. A typical result is shown in Figure 17 where ψ is taken to be 10° and maximum growth rates are shown for several values of θ . A decrease in θ from 80° results in a decrease in the maximum value of the growth rate for low Mach numbers. For all

values of θ the trend in the maximum growth rate with Mach number is similar. For the subsonic mode and its slow supersonic continuation the growth rates decrease by a factor of five to ten with Mach number and then level off. The growth rates of the fast supersonic modes, which appear at M_* , increase slightly and then decrease with increasing Mach number. The growth rate for $\theta = 80^\circ$ is always greater than the growth rates of the other cases. At $M = 2$, the growth rate of the $\theta = 80^\circ$ case is comparable to the growth rate of the $\theta = 0^\circ$ case at $M = 0$.

It was further found, using a flame sheet model, that the addition of combustion had important, and complex, effects on the flow stability (Jackson and Grosch, 1990b). A set of typical results is shown in Figure 18. The maximum growth rate as a function of M with $\beta_T = 2$, $\phi = 1$ and various values of the heat release parameter, β is plotted in Figure 18a. Figure 18b contains similar results, but with β fixed at a value of 2 and $\phi = 0.5, 1.0, 2.0$. The results in Figure 18a show that the maximum growth rates of the slow modes are strictly increasing and those of the fast modes are strictly decreasing with increasing β at zero Mach number. The results of Figure 18b show that increasing ϕ yields an increased in the growth rates of the fast modes while decreasing those of the slow modes. However, the growth rates of both are independent of ϕ at higher Mach number.

Finally, as will be discussed in more detail in Section 3.5, Jackson and Grosch (1990b) found that the addition of heat from the reaction could cause a transition from convective to absolute instability without any backflow.

3.4 The Convective Mach Number

In order to correlate experimental results, a number of experimentalists have used a heuristically defined "convective Mach number". This idea, first introduced by Bogdanoff (1983) for compressible flows, has permeated much of the experimental work on non-reacting compressible mixing layers. The convective Mach number, M_c , has been used to correlate the reduction in growth rate (Papamoschou and Roshko, 1986, 1988) and the reduction in the Reynolds stresses (Elliott and Samimy, 1990; Samimy and Elliot, 1990; Goebel and Dutton, 1991) which are observed to occur in this flow as the Mach number is increased. Several different definitions of a convective Mach number have been advanced. One approach is to define a Mach number in a moving frame of reference which is fixed either to the large scale structures of the mixing layer (Bogdanoff, 1983; Papamoschou and Roshko, 1986, 1988) or to the most unstable wave (Zhuang, Kubota and Dimotakis, 1988). These definitions were for unbounded flows. Tam and Hu (1988, 1991) have applied the same ideas to the non-reacting mixing layer in a channel.

Jackson and Grosch (1990a) defined a convective Mach number in terms of a generalization of the M_* defined in equation (26). They argued that M_* marked the transition between two different flow regimes: if $M < M_*$ it is possible to have disturbances which are subsonic in both streams but if $M > M_*$ only disturbances which are supersonic in either or both streams are possible. They derived the equations of linear stability theory for the flow of multispecies streams of gas and showed that the c_{\pm} can be rewritten in terms of the mixture quantities as

$$c_+ = 1 - 1/M, \quad (61)$$

$$c_- = \beta_U + 1/M \sqrt{\beta_\rho / \beta_\gamma}, \quad (62)$$

where M is the mixture Mach number at $\eta = +\infty$ and β_ρ and β_γ are defined in terms of the mixture quantities at $\pm\infty$ by

$$\beta_\rho = \rho(-\infty)/\rho(\infty), \quad (63)$$

and

$$\beta_\gamma = \gamma(-\infty)/\gamma(\infty). \quad (64)$$

Thus Jackson and Grosch (1990a) defined a convective Mach number for a multi-species gas as

$$M_c = M(1 - \beta_U)/(1 + \sqrt{\beta_\gamma/\beta_\rho}). \quad (65)$$

The other definitions of the the convective Mach number for a multispecies gas are (in the notation used here): that of Bogdanoff (1983)

$$M_c = M(1 - \beta_U)/(1 + 1/\sqrt{\beta_\rho})\beta_\gamma^{1/4}, \quad (66)$$

Papamoschou and Roshko (1986, 1988)

$$M_c = M(1 - \beta_U)/(1 + 1/\sqrt{\beta_\rho}), \quad (67)$$

and Zhuang, Kubota, and Dimotakis (1988)

$$M_c = M(1 - c_{ph}), \quad (68)$$

where c_{ph} is the phase speed of the most unstable mode from linear stability theory. For a single species gas $\beta_\gamma = 1$ and the definition of the convective Mach number of Jackson and Grosch, Bogdanoff, and Papamoschou and Roshko are equal. For most multi-species gases β_γ is close to one and all three definitions yield values of the convective Mach number which are nearly equal. These definitions are for two dimensional disturbances propagating in the direction of the mean flow. If the disturbances are oblique waves propagating at an angle θ to the mean flow direction, the definition of M_c can be generalized by replacing the free stream Mach number M by the effective Mach number $M \cos\theta$.

The convective Mach number definitions of Bogdanoff and Papamoschou and Roshko are based on the speed of the large scale structures and that Zhuang, Kubota and Dimotakis is based on the speed of the most unstable wave. Both concepts refer to events within the mixing layer. The reaction may be expected to change the speed of both the large scale structures and the most unstable wave. Thus the definitions of M_c should be different for a reacting as compared to a non-reacting flow. The definition of Jackson and Grosch is based on the sonic speeds in the far field. The far field is chemically frozen so their definition of M_c is independent of the reaction.

Jackson and Grosch (1990b) plotted R , the maximum growth rate at an M_c (normalized by that at $M_c = 0$) versus M_c as obtained from the results of spatial stability calculations for a non-reacting compressible mixing layer using the Tanh, Lock and Sutherland models. In addition, the results included the data for three values of the dimensionless temperature of the slow stream, $\beta_U = 0.5, 1, 2$. They showed, that with these scalings, the data collapsed onto essentially a single curve for $M_c < 1$, and a narrow band for $M_c > 1$ with additional unstable modes appear around $M_c = 1$. This result is similar to that obtained by Ragab and Wu (1988) using a single thermodynamic

model but not including the second supersonic modes and using Bogdanoff's heuristic definition of the convective Mach number.

Although the convective Mach number does correlate the results of stability calculations, its main use has been in correlating experimental results and, in this role, there have been certain problems associated with its use for supersonic mixing layers. In the interpretation of experimental results two convective Mach numbers are computed, one using the difference in speed between the fast stream and the speed of the large scale structures (the "fast" one) and the other using the difference in speed between the slow stream and the speed of the large scale structures (the "slow" one). Assuming that there is a stagnation point between each pair of structures, an argument based on isentropic pressure matching leads to the result that the two convective Mach numbers should be equal, or nearly so.

Figure 19 contains curves of the normalized maximum growth rate versus the effective convective Mach number for the Tanh model with $\beta_T = 0.5$ and $\beta_U = 0$ and for the instability waves traveling at an angle θ to the mean flow direction. These curves are based on the numerical calculations of Jackson and Grosch (1989). Results are shown for $\theta = 0^\circ, 20^\circ, 40^\circ, 60^\circ$. For angles of propagation greater than 60° it was found (Jackson and Grosch, 1989) that the maximum growth rate begins to decrease with increasing angles of propagation. The data points shown in this figure are taken from the experimental results of Papamoschou and Roshko (1988), Samimy and Elliot (1990), Clemens and Mungal (1990), and Hall, Dimotakis and Rosemann (1991). The data, taken from these papers, are summarized in Tables 1 through 4. The trends in both the theoretical and experimental results are roughly similar although there is a great deal of spread in the data and no single theoretical curve "fits" all of the data.

The results of some recent experiments have also cast doubt on the relevance of the concept of a convective Mach number. The measurements of Papamoschou (1989) yielded convection speeds which were very close to one or the other of the free stream speeds. Thus the "fast" and "slow" convective Mach numbers were very different. In another experiment (Hall, Dimotakis and Rosemann, 1991) large scale coherent structures were in general *not* seen in Schlieren photographs. However the presence of such structures was inferred from the existence of traveling shock and expansion waves in the low speed side of the flow. The inferred convection speeds of these structures were reported to be much higher than would be predicted for the "fast" convective Mach number. Samimy, Reeder, and Elliot (1992) reported measurements of the convective speed, U_c , of individual structures in compressible mixing layers for two cases. In both cases the fast stream was supersonic and the slow stream subsonic. These speeds were obtained from the signals of a pair of pressure probes in the layer. Their paper contains histograms of the measured U_c at various positions in the mixing layer for two cases. For case 1 the theoretical value of U_c was 352 m/sec and for case 2 it was 428 m/sec, both obtained from Bogdanoff's definition of the convective Mach number. In both cases the results of the measurements showed that there was not a single value of U_c but rather a wide range of values. On the centerline the mean of the distribution was close to the theoretical value but the range was appreciable, about $\pm 40\%$ of the mean. Off the centerline, the mean was 5% to 10% lower than on the centerline and the range was equally large (about 40%).

These experimental results suggest that the convective Mach number can be regarded as an indication of the importance of compressibility effects but may not be very useful beyond that. It is suggested that the observation of convection speeds very close to

one or the other of the free stream speeds (Papamoschou, 1989) may be a reflection of the existence of instability waves with both fast and slow phase speeds. Similarly, the observations of Hall, Dimotakis and Rosemann (1991) could be a nonlinear form of the fast instability waves which are subsonic in the fast stream and are supersonic in the slow stream. Linear stability theory predicts that the disturbances are constant amplitude outgoing waves in the slow stream and the nonlinear form of these might be the shock-rarefaction wave pattern observed. It would be desirable to examine the data in the light of this theory. Numerical experiments could probably provide a definitive test of this hypothesis.

3.5 Convective/Absolute Instabilities

In the stability problem, the eigenvalue is a zero of the characteristic equation relating the wavenumber α and the frequency ω at fixed Mach number. Since $\alpha(\omega)$ has a square root branch point singularity at a zero of the complex group velocity $d\omega/d\alpha$ (Briggs, 1964; Gaster, 1968), transition from convective to absolute instability occurs when the zero lies on the real ω axis. Therefore Jackson and Grosch (1990b), using a flame sheet model, and Hu, Jackson, Lasseigne, and Grosch (1993), using finite rate chemistry, choose ω to be real, α to be complex, and carried out a numerical search for a zero of $d\omega/d\alpha$. It was shown by Jackson and Grosch (1990b) that the fast branch was convectively unstable while the slow branch undergoes a transition from convective to absolute instability.

Qualitatively similar behavior was found for both the flame sheet and finite rate models; in particular (Hu, et al, 1993) a plot of α_i versus α_r as the real frequency ω varies continuously has (Figure 20) a saddle point for the speed of the slow stream, β_U , between 0.014 and 0.016 showing the presence of a square root branch point singularity due to a transition from convective to absolute instability. Figure 21 (Hu, et al, 1993) shows the effect of varying the temperature at $-\infty$, β_T , and the heat release parameter, β , on the boundary between the regions of convective and absolute instability in the $\beta_U - M$ plane. With β fixed, decreasing β_T , that is cooling the flow at $-\infty$, results in an increase in the range of β_U for which the flow is absolutely unstable. Similarly, increasing the heat release parameter, β , with fixed temperature at $-\infty$ also increases the range of β_U over which the flow is absolutely unstable. Although the range of β_U over which the flow is absolutely unstable is largest for subsonic flow, sufficient cooling at $-\infty$ and/or heat release can cause an absolute instability in supersonic mixing layers.

Similar calculations were made to determine how obliquely traveling disturbances affects the convective/absolute instability transition. The results presented in Figure 22 (taken from those of Hu, et al, 1993) show that increasing the angle of propagation with respect to the mean flow direction, θ , increases the range of β_U over which the reacting flow is absolutely unstable, at least over the parameter ranges examined in their study. This effect seems to be a purely kinematic one in that the wave propagating at an oblique angle relative to the mean flow direction "sees" a flow with a lower Mach number. This is evident from the scaling to an effective Mach number, $M \cos\theta$, which collapses all of the curves for the oblique disturbances onto essentially a single curve, corresponding that for $\theta = 0^\circ$, see Figure 23.

The results of Hu, et al (1993) show that, whatever the values of the other parameters, the reacting mixing layer will be convectively, rather than absolutely, unstable at sufficiently large Mach number unless there is a backflow. It is easily shown that,

for any β and ϕ , if M is large enough the temperature distribution in the layer will be approximated by that of a non-reacting flow and this requires a negative β_U for an absolute instability. Thus large Mach numbers cause the flow to be convectively, rather than absolutely, unstable. It was also found that cooling the slow stream (decreasing β_T) and increasing the heat release (increasing β) both caused an increase in the range of β_U and Mach number over which an absolute instability existed. These results suggested that it was the magnitude of the temperature gradient induced by the flame which must be large for the absolute instability to occur.

Hu, et al (1993) also used a complementary approach to investigate the transition from convective to absolute instability, namely to examine the response, $I(x, t)$, of the flow to an impulse in space and time (see Huerre and Monkewitz 1985, and the references cited therein). The impulse generates a wave packet in the (x, t) plane with the real part of I the wave packet and its absolute value the envelope. An asymptotic expansion of the impulse response for large time can be determined by the method of steepest descent (Gaster, 1981, 1982) The leading term in the expansion is

$$I = \left[\frac{2\pi}{(d^2\omega/d\alpha^2)t} \right]_{\alpha=\alpha^*}^{1/2} e^{\Sigma t} [1 + O(t^{-1})], \quad (69)$$

where

$$\Sigma = i(\alpha^* \frac{x}{t} - \omega(\alpha^*)). \quad (70)$$

The value of α^* was found from the requirement that the rays in the wave packet had constant real values of the group velocity, C_g . This gave

$$C_g = \left[\frac{d\omega}{d\alpha} \right]_{\alpha=\alpha^*} = \frac{x}{t}. \quad (71)$$

Sets of $\{\alpha^*, \omega(\alpha^*)\}$ pairs which satisfy this equation were then found.

Two, generally distinct, wave packets were found by Hu, et al: the first was made up of the unstable modes of the slow branch, which are absolutely unstable in certain parameter ranges, and the second was made up of the unstable modes of the fast branch which are always convectively unstable. The real part of Σ , the temporal growth rate along the rays, as found by Hu, et al is plotted in Figure 24 for both the fast and slow unstable branches at $M = 0$ for various values of β . As β increases, the maximum of the real part of Σ for the slow branch decreases and the range of x/t for which the real part of Σ is positive decreases. For the fast branch, the maximum growth rate increases by a small amount, and the range of unstable frequencies increases. Figure 24b is an enlargement of Figure 24a near $x/t = 0$. The real part of Σ goes to zero at x/t slightly above 0.03 for $\beta = 0.5$. For $\beta = 1.38$, it is zero at $x/t = 0$, and for $\beta = 4$, it is zero at $x/t \approx -0.035$. The fact that the real part of Σ is positive for a range of negative values of x/t shows that the wave packet is traveling *both* upstream and downstream and therefore that the flow is absolutely unstable. It is important to note that the growth rates in the region of $x/t < 0$ are small compared to the maximum growth rate. Consequently the upstream propagating portion of the wave packet grows slowly compared to downstream propagating part.

The effect of increasing the Mach number on the temporal growth rate along the rays is shown in Figure 25 where the variation of Σ with x/t for $\beta = 4$ and various Mach numbers is shown. The temporal growth rates for the fast branch are only slightly effected by the change in M from 0 to 0.8 with a small decrease in the maximum and

the range of x/t over which it is positive. There is a much greater effect on the slow branch. The peak value decreases by more than a factor of 2 as M increases to 0.8 and the range of x/t over which this branch is unstable decreases. For $M = 0.8$ the slow branch only has a positive growth rate for $x/t > 0$, indicating that there is no absolute instability at this Mach number.

Typical wave packets, as computed by Hu, et al, resulting from the impulse with $M = 0.4$ and $\beta = 4$ are shown at (a) $t = 100$ and (b) $t = 500$ in Figure 26. In each figure there are a pair of wave packets: one is a fast packet containing the unstable modes of the fast branch and the other a slow packet containing the unstable mode of the slow branch. As the pair evolves in time, they move apart because of the substantial differences in their group velocities. At $t = 100$ (26a) the slow packet is somewhat larger than the fast packet and clearly exists in a region of $x < 0$, showing the absolute instability. At $t = 500$ (26b) both packets have grown, spread, and moved apart. The notation, $X10$, close to the slow packet means that the amplitude of the slow packet, but not that of the fast packet, has been multiplied by a factor of 10 in order that it be visible on this scale. In 26b the fast packet is much larger than the slow packet because of its greater growth rate. The slow wave packet extends into the region $x < 0$, but because of the scaling, it is difficult to see this on the figure. As time increases, the slow packet will continue to grow, but at a much slower rate than the fast packet, and spread both upstream and downstream. However the upstream propagation is very slow. These results are for $\beta_T = 0.5$. Hu, et al state that similar results were also found at other values of β_T .

These wave packet calculations showed that when the reacting shear layer is absolutely unstable it is *weakly* unstable. That is, with increasing Mach number from zero and a fixed rate of heat release, the absolute instability becomes progressively weaker in that the range of negative x/t over which the growth rate is non-negative grows smaller and the growth rate in this region and the speed of the upstream traveling waves also becomes smaller. Thus a wave packet will grow and spread throughout the entire domain, but it may take a long time for this to happen.

4. Concluding Remarks

The results of the numerics and asymptotics show that the reacting compressible mixing layer has a rather complex structure. In particular, the ignition point and the location of the diffusion flame in the layer are sensitive to the parameters of the flow. All of these results (numeric as well as asymptotic) were found while using the simplifying assumptions of $Pr = 1$ and a linear viscosity-temperature relation. It is highly desirable to determine to what extent these results are dependent on the simplifying assumptions for the flow properties. Would the use of $Pr = 0.72$ and a Sutherland viscosity law, say, result in *qualitative* changes in the results or merely *quantitative* ones? It is certainly expected that there would be quantitative changes in the results and it is desirable to find out how large these would be.

The structure of the reacting compressible mixing layer has been studied using a very simple model for the combustion process: fuel and oxidizer undergoing a one step irreversible reaction. It is clear from calculations using more complex, and realistic, combustion models (see for example the calculations of Birkan and Law (1988) for counterflow flames) that these models can yield a richer and more complex structure than that found for the one step irreversible model. It is desirable to re-do the analysis

of the structure of the reacting compressible shear layer using at least one, and possibly more, of the more realistic combustion models. Candidate models include the two step reversible model of Rogers and Chinitz (1983), the three step irreversible model of Birkan and Law (1988), and the three and two step models of Balakrishnan (1992).

The experimental results cited above suggest that the convective Mach number can be regarded as an indication of the importance of compressibility effects but may not be very useful beyond that. Carefully designed numerical experiments may be able to shed additional light on the role of the convective Mach number. In particular, they could be used to look for "structures" with convection speeds very close to one or the other of the free stream speeds, as observed by Papamoschou (1989). One could test the hypothesis that they are a reflection of the existence of instability waves with both fast and slow phase speeds. Again, are Hall, Dimotakis and Rosemann (1991) observing a nonlinear form of fast instability waves which are subsonic in the fast stream and supersonic in the slow stream? Linear stability theory predicts that there are disturbances which are constant amplitude outgoing waves in the slow stream. The nonlinear form of these might be the shock-rarefaction wave pattern observed. Finally, numerical experiments might be used to examine the nonlinear form of the absolutely unstable waves predicted using linear theory. Very careful calculations would be required in order to minimize the effects of numerical dissipation. The role of physical damping on the convective/absolute transition also needs to be investigated.

Most of the theoretical studies of structure and stability have dealt with compressible mixing layers. While this is a useful model, these studies should be extended to other flow configurations, perhaps compressible jets.

References

- Artola, M. and Majda, A.J. 1987 "Nonlinear Development of Instabilities in Supersonic Vortex Sheets". *Physica D*, 28, 253-281.
- Balakrishnan, G. 1992 "Studies of Hydrogen-Air Diffusion Flames and of Compressibility Effects Related to High-Speed Propulsion". PhD Dissertation, University of California, San Diego.
- Balsa, T.F. and Goldstein, M.E. 1990 "On the Instabilities of Supersonic Mixing Layers: A High Mach Number Asymptotic Theory". *J. Fluid Mech.*, 216, 585-611.
- Beach, H.L. 1992 "Supersonic Combustion Status and Issues". In *Major Research Topics in Combustion*, M.Y. Hussaini, A. Kumar, R.G. Voigt, (eds.) Springer-Verlag, 1-20.
- Birkan, M.A. and Law, C.K. 1988 "Asymptotic Structure and Extinction of Diffusion Flames with Chain Mechanism". *Twenty-Second Symposium (International) on Combustion*, The Combustion Institute, 127-146.
- Blumen, W., Drazin, P.G. and Billings, D.F. 1975 "Shear Layer Instability of an Inviscid Compressible Fluid". Part 2, *J. Fluid Mech.*, 71, 305-316.
- Bogdanoff, D.W. 1983 "Compressibility Effects in Turbulent Shear Layers". *AIAA Journal*, 21, 926-927.
- Briggs, R.J. 1964 *Electron-Stream Interaction with Plasmas*, Research Monograph No. 29, MIT Press, Cambridge, Mass.
- Brown, G.L. and Roshko, A. 1974 "On Density Effects and Large Structure in Turbulent Mixing Layers". *J. Fluid Mech.*, 64, 775-816.
- Chimonas, G. 1970 "The Extension of the Miles-Howard Theorem to Compressible Fluids". *J. Fluid Mech.*, 43, 833-836.
- Chinzei, N., Masuya, G., Komuro, T., Murakami, A. and Kudou, D. 1986 "Spreading of Two-Stream Supersonic Turbulent Mixing Layers". *Phys. Fluids*, 29, 1345-1347.
- Clemens, N.T. and Mungal, M.G. 1992 "Two- and Three-Dimensional Effects in the Supersonic Mixing Layer". *AIAA Paper 90-1978*.
- Clemens, N.T. 1992 "An Experimental Investigation of Scalar Mixing in Supersonic Turbulent Shear Layers". *HTGL Report T-274*, Mechanical Engineering Department, Stanford University.
- Djordjevic, V.D. and Redekopp, L.G. 1988 "Linear Stability Analysis of Nonhomotropic, Inviscid, Compressible Flows". *Physics of Fluids*, 31, 3239-3245.

- Drazin, P.G. and Howard, L.N. 1962 "Shear Layer Instability of an Inviscid Compressible Fluid. Part 2". *J. Fluid Mech.*, 71, 305-316.
- Drazin, P.G. and Reid, W.H. 1984 *Hydrodynamic Stability*, Cambridge University Press, Cambridge.
- Drummond, J.P. and Mukunda, H.S. 1988 "A Numerical Study of Mixing Enhancement in Supersonic Reacting Flow Fields". AIAA Paper 88-3260.
- Drummond, J.P., Carpenter, M.H., Riggins, D.W. and Adams, M.S. 1989 "Mixing Enhancement in a Supersonic Combustor". AIAA Paper 89-2794.
- Elliott, G.S. and Samimy, M. 1990 "Compressibility Effects in Free Shear Layers". *Physics of Fluids A*, 2, 1231.
- Gaster, M. 1968 "Growth of Disturbances in Both Space and Time". *Physics of Fluids*, 11, 723-727.
- Gaster, M. 1981 "Propagation of Linear Wave Packets in Laminar Boundary Layers". *AIAA Journal*, 19, 419-423.
- Gaster, M. 1982 "Estimates of the Errors Incurred in Various Asymptotic Representations of Wave Packets". *J. Fluid Mech.*, 121, 365-377.
- Goebel, S.G. and Dutton, J.C. 1991 "Experimental Study of Compressible Turbulent Mixing Layers". *AIAA Journal*, 29, 538-546.
- Grosch, C.E. and Jackson, T.L. 1991a "Inviscid Spatial Stability of a Three Dimensional Compressible Mixing Layer". *J. Fluid Mech.*, 231, 35-50.
- Grosch, C.E. and Jackson, T.L. 1991b "Ignition and Structure of a Laminar Diffusion Flame in a Compressible Mixing Layer with Finite Rate Chemistry". *Physics of Fluids A*, 3, 3087-3097.
- Grosch, C.E., Jackson, T.L., Klein, R., Majda, A. and Papageorgiou, D.T. 1991 "The Inviscid Discrete Eigenvalue Spectrum of the Compressible Mixing Layer". Unpublished manuscript.
- Guirguis, R.H. 1988 "Mixing Enhancement in Supersonic Shear Layers: III. Effect of Convective Mach Number". AIAA Paper 88-0701.
- Hall, J.L., Dimotakis, P.E. and Rosemann, H. 1991 "Experiments in Non-Reacting Compressible Shear Layers". AIAA Paper 91-0629.
- Ho, C. M. and Huerre, P. 1984 *Perturbed Free Shear Layers*. *Annual Review of Fluid Mechanics*. 16, 365-424.
- Hu, F.Q. 1992 Personal Communication.
- Hu, F.Q., Jackson, T.L., Lasseigne, G.L. and Grosch, C.E. 1993 "Absolute/Convective Instabilities and Their Associated Wave Packets in a Compressible Reacting Mixing Layer". *Physics of Fluids A*, 5, 901-915.

- Huerre, P. and Monkewitz, P.A. 1990 Local and Global Instabilities in Spatially Developing Flows. *Annual Review of Fluid Mechanics*. 22, 473-537.
- Jackson, T.L. 1992 "Stability of Laminar Diffusion Flames in Compressible Mixing Layers. In *Major Research Topics in Combustion*, M.Y. Hussaini, A. Kumar, R.G. Voigt, (eds.) Springer-Verlag, 131-161.
- Jackson, T.L. and Grosch, C.E. 1989 "Inviscid Spatial Stability of a Compressible Mixing Layer". *J. Fluid Mech.*, 208, 609-637.
- Jackson, T.L. and Grosch, C.E. 1990a "Absolute/Convective Instabilities and the Convective Mach Number in a Compressible Mixing Layer". *Physics of Fluids A*, 2, 949-954.
- Jackson, T.L. and Grosch, C.E. 1990b "Inviscid Spatial Stability of a Compressible Mixing Layer. Part 2. The Flame Sheet Model". *J. Fluid Mech.*, 217, 391-420.
- Jackson, T.L. and Grosch, C.E. 1991 "Inviscid Spatial Stability of a Compressible Mixing Layer. Part 3. Effect of Thermodynamics". *J. Fluid Mech.*, 224, 159-175.
- Jackson, T.L. and Hussaini, M.Y. 1988 "An Asymptotic Analysis of Supersonic Reacting Mixing Layers." *Comb. Sci. Tech.* 57, 129-140.
- Lees, L. and Lin, C.C. 1946 "Investigation of the Stability of the Laminar Boundary Layer in a Compressible Fluid". *NACA Tech. Note* 1115.
- Lele, S.K. 1989 "Direct Numerical Simulation of Compressible Free Shear Layer Flows". *AIAA* 89-0374.
- Linan, A. and Crespo, A. 1976 "An Asymptotic Analysis of Unsteady Diffusion Flames for Large Activation Energies". *Comb. Sci. Tech.*, 14, 95-117.
- Miles, J. W. 1958 "On the Disturbed Motion of a Plane Vortex Sheet". *J. Fluid Mech.*, 4, 538-552.
- Papamoschou, D. and Roshko, A. 1986 "Observations of Supersonic Free-Shear Layers". *AIAA Paper* 86-0162.
- Papamoschou, D. and Roshko, A. 1988 "The Compressible Turbulent Shear Layer: An Experimental Study". *J. Fluid Mech.*, 197, 453-477.
- Papamoschou, D. 1989 "Structure of the Compressible Turbulent Shear Layer". *AIAA Paper* 89-0126.
- Planche, O.H. and Reynolds, W.C. 1991 "Compressibility Effect on the Supersonic Reacting Mixing Layer". *AIAA Paper* 91-0739.
- Ragab, S.A. and Wu, J.L. 1988 "Instabilities in the Free Shear Layer Formed by Two Supersonic Streams". *AIAA Paper* 88-0038.

- Rogers, R.C. and Chinitz, W. 1983 "Using a Global Hydrogen-Air Combustion Model in Turbulent Reacting Flow Calculations". AIAA Journal, 21, 586-592.
- Samimy, M. and Elliott, G.S. 1990 "Effects of Compressibility on the Characteristics of Free Shear Layers". AIAA Journal, 28, 439-445.
- Samimy, M., Reeder, M.F. and Elliott, G.S. 1992 "Compressibility Effects on Large Structures in Free Shear Flows." Physics of Fluids A, 4, 1251-1258.
- Sandham, N. and Reynolds, W. 1989 "The Compressible Mixing Layer: Linear Theory and Direct Simulation". AIAA Paper 89-0371.
- Shin, D. and Ferziger, J. 1990 "Linear Stability of the Reacting Mixing Layer". AIAA Paper 90-0268.
- Shin, D.S. and Ferziger, J.H. 1991 "Stability of Compressible Reacting Mixing Layer". AIAA Paper 91-0372.
- Tam, C.K.W. and Hu, F.Q. 1988 "Instabilities of Supersonic Mixing Layers Inside a Rectangular Channel". AIAA Paper 88-3675.
- Tam, C.K.W. and Hu, F.Q. 1991 "Resonant Instability of Ducted Free Supersonic Mixing Layers Induced by Periodic Mach Waves". J. Fluid Mech., 229, 65-85.
- Zhuang, M., Kubota, T. and Dimotakis, P.E. 1988 "On the Instability of Inviscid, Compressible Free Shear Layers". AIAA Paper 88-3538.

**DATA FOR CONVECTIVE MACH NUMBER
GROWTH RATE CORRELLATION**

Table 1 : Data of Papamoschou and Roshko, J. Fluid Mech. 197, 453,1988

Case	Gas 1	Gas 2	M	β_U	β_ρ	β_γ	M_c	Ratio
1	Ar	Ar	3.4	0.81	0.43	1.00	0.26	1.00
2	N_2	N_2	3.1	0.74	0.54	1.00	0.34	0.70
3	N_2	Ar	2.8	0.75	1.80	1.19	0.39	0.71
4	N_2	Ar	3.2	0.67	1.20	1.19	0.53	0.50
5	He	N_2	1.7	0.54	9.20	0.84	0.60	0.22
6	Ar	Ar	3.1	0.13	0.24	1.00	0.89	0.23
7	He	N_2	2.6	0.42	5.50	0.84	1.03	0.28
8	He	N_2	3.4	0.29	2.20	0.84	1.39	0.18
9	He	Ar	3.1	0.04	2.40	1.00	1.81	0.23

Table 2 : Data of Samimy and Elliot, AIAA J. 28, 439, 1990

Case	Gas 1	Gas 2	M_1	M_2	β_U	β_ρ	β_γ	M_c	Ratio
1	Air	Air	1.80	0.51	0.36	0.64	1.00	0.512	0.96
2	Air	Air	1.96	0.37	0.25	9.58	1.00	1.111	0.65

Table 3 : Data of Clemens and Mungal, AIAA-90-1978

Case	Gas 1	Gas 2	M_1	M_2	β_U	β_ρ	β_γ	M_c	Ratio
1	Air	Air	1.64	0.91	0.63	0.77	1.00	0.284	0.59
2	Air	Air	1.97	0.47	0.28	0.59	1.00	0.616	0.41
3	Air	Ar	2.15	0.38	0.22	0.79	1.19	0.753	0.31

Table 4 : Data of Hall, Dimotakis and Rosemann, AIAA-91-0629

Case	Gas 1	Gas 2	M_1	M_2	β_U	β_p	β_γ	M_c	Ratio
1	He	Ar	1.50	0.35	0.096	5.950	1.00	0.962	0.233
2	He	N_2	1.48	0.30	0.092	4.120	0.84	0.926	0.274
3	N_2	N_2	1.46	0.29	0.235	0.713	1.00	0.511	0.570
4	N_2	33% He 67% Ar	1.48	0.44	0.385	0.706	1.19	0.396	0.630
5	N_2	60% He 40% Ar	1.48	0.42	0.445	0.484	1.19	0.320	0.680
6	N_2	75% He 25% Ar	1.47	0.36	0.459	0.338	1.19	0.276	0.780
7	N_2	90% He 10% Ar	1.48	0.28	0.469	0.194	1.19	0.226	0.678
8	N_2	He	1.48	0.23	0.510	0.101	1.19	0.164	0.660
9	Ar	He	1.50	0.23	0.636	0.058	1.00	0.106	0.597
10	N_2	33% He 67% Ar	0.59	0.27	0.510	0.958	1.19	0.137	0.918
11	N_2	He	0.65	0.10	0.462	0.132	1.19	0.087	0.907

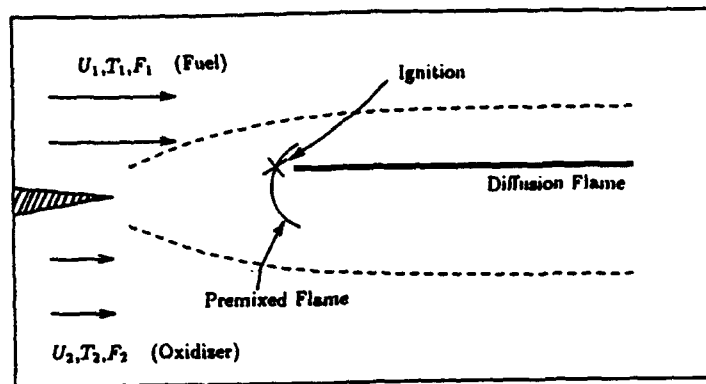


Figure 1. Schematic showing the reacting mixing layer, with the adiabatic flame temperature greater than T_1 and T_2 .

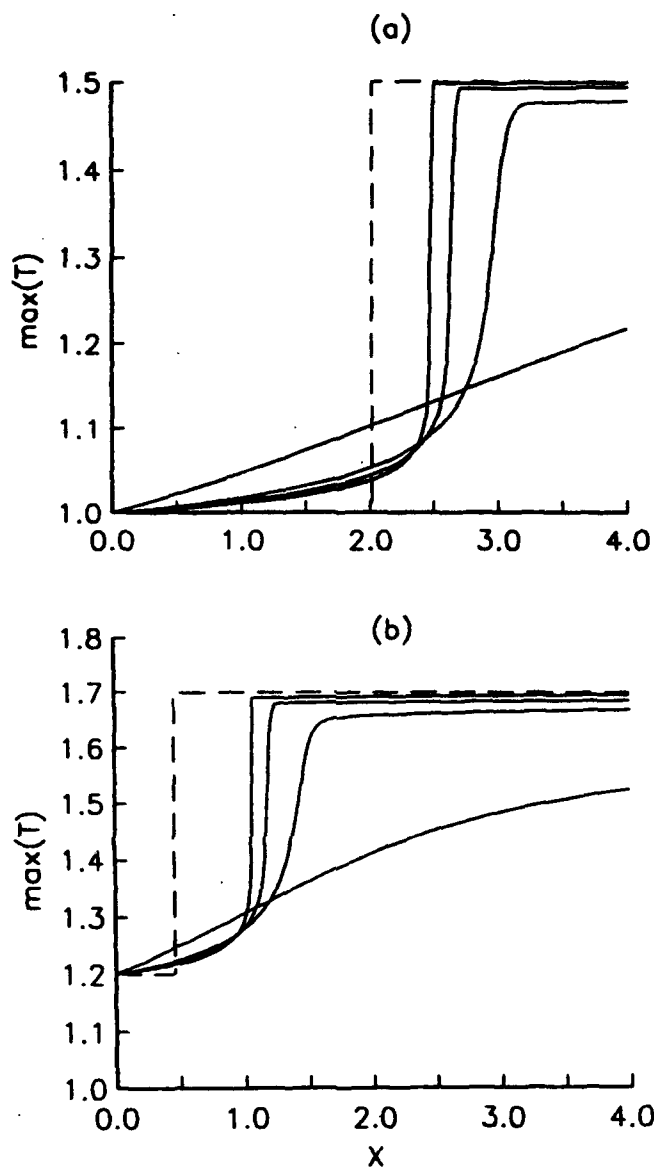


Figure 2. Plot of the maximum temperature in η versus x for $\beta_U = 0$, $\beta_T = \beta = \phi = 1$ with (a) $M = 0$, and (b) $M = 2$. In both graphs the Zeldovich number increases from right to left with $Ze = 10, 30, 40$, and 50 . The dashed line corresponds to the solution in the infinite Zeldovich limit.

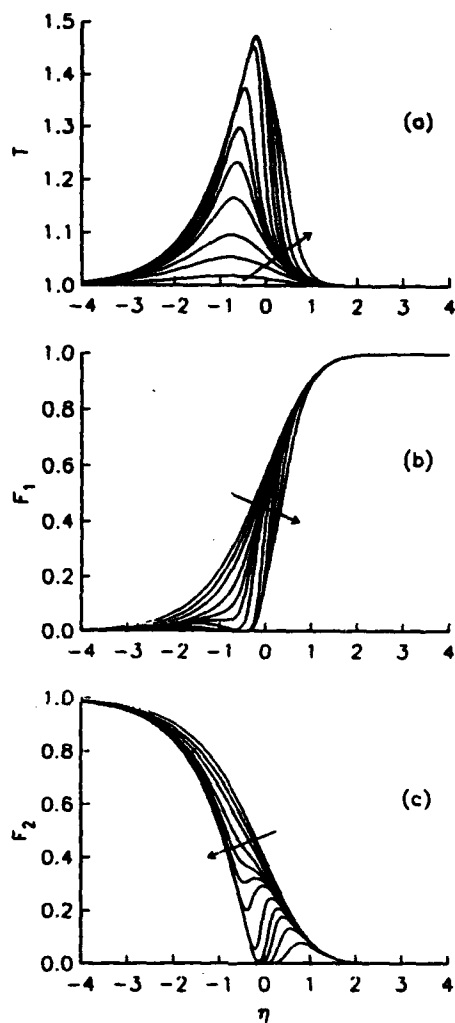


Figure 3. Plot of (a) temperature, (b) F_1 mass fraction, (c) F_2 mass fraction versus η for $M = 0$, $\beta_U = 0$, $\beta_T = \beta = \phi = 1$, $Ze = 30$. Here, the arrow denotes increasing x , with $x = 1, 2, 2.5, 2.8, 2.9, 2.95, 3, 3.1, 3.2, 3.3, 3.5, 4$.

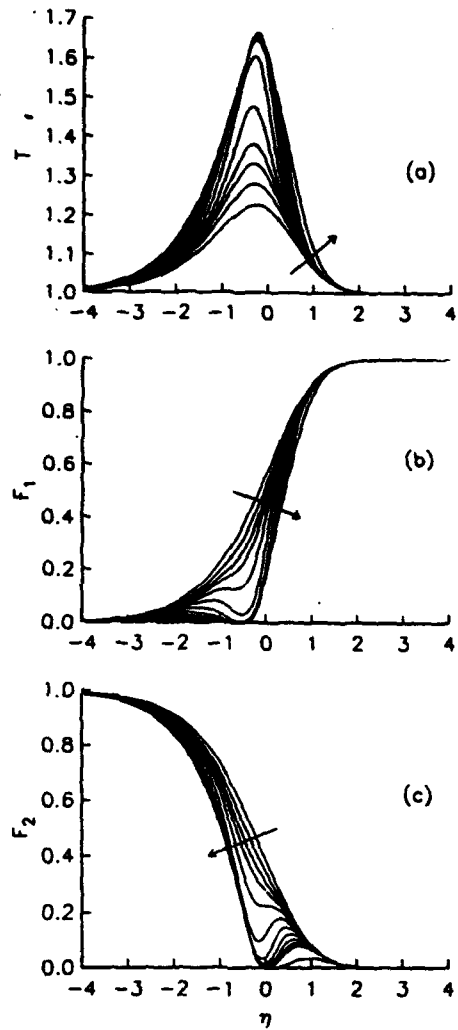


Figure 4. Plot of (a) temperature, (b) F_1 mass fraction, (c) F_2 mass fraction versus η for $M = 2$, $\beta_U = 0$, $\beta_T = \beta = \phi = 1$, $Ze = 30$. Here, the arrow denotes increasing x , with $x = 0.5, 1, 1.2, 1.3, 1.4, 1.5, 1.6, 1.7, 1.8, 1.9, 2, 3$.

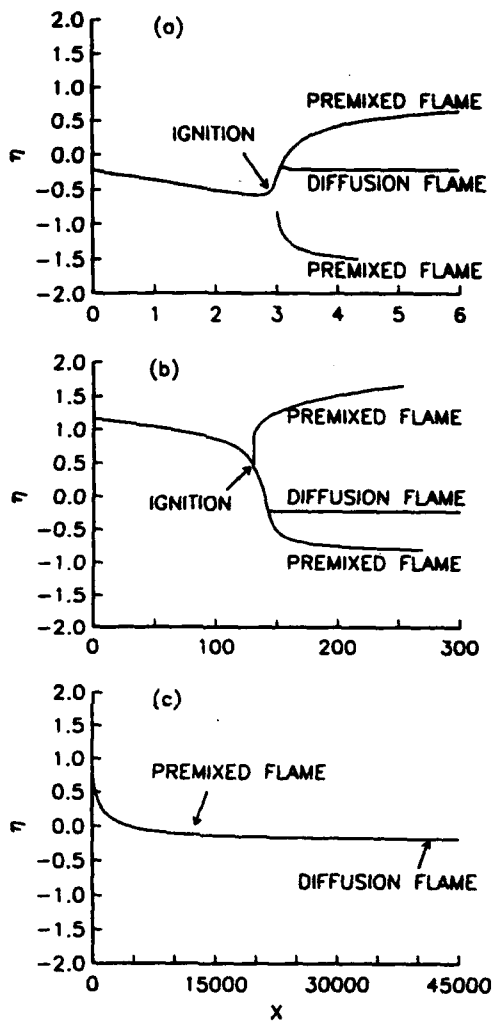


Figure 5. Plot of the loci in the (x, η) plane of the maxima of Ω for $M = \beta_U = 0$, $\phi = 1$, $Ze = 30$, and (a) $\beta_T = \beta = 1$; (b) $\beta_T = 0.5$, $\beta = 1.5$; and (c) $\beta_T = 0.5$, $\beta = 0.4$.

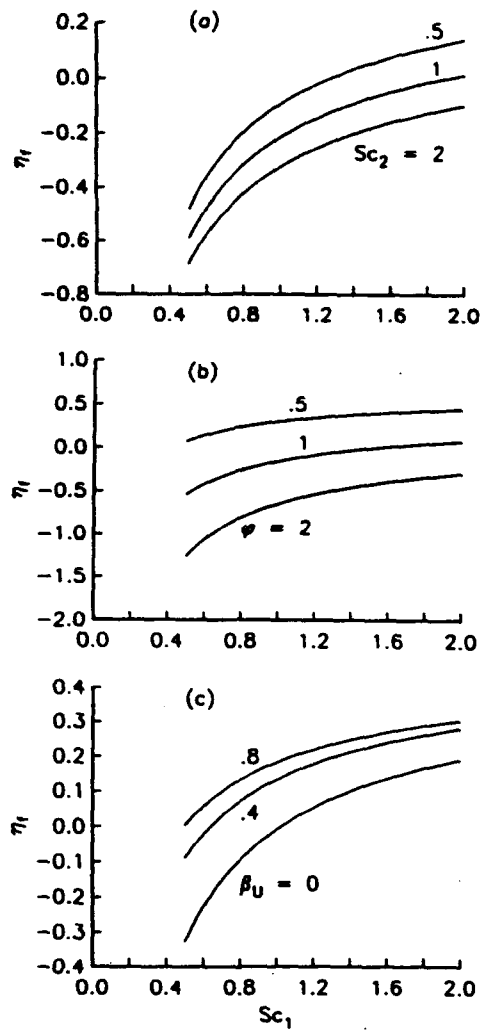


Figure 6. Plot of the flame location η_f versus Sc_1 : (a) $\beta_U = 0$, $\phi = 1$, $Sc_2 = .5, 1, 2$; (b) $\beta_U = 0$, $\phi = .5, 1, 2$, $Sc_2 = .7$; (c) $\beta_U = 0$, $\phi = .4, .8$, $Sc_2 = .7$.

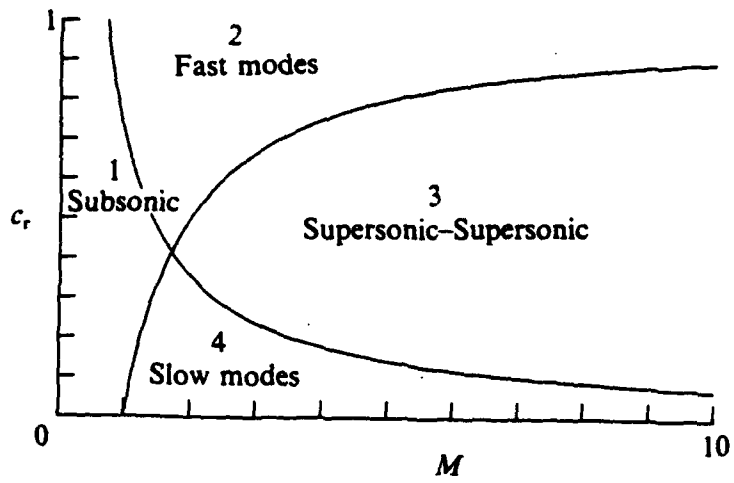


Figure 7. Plots of the sonic speeds c_{\pm} versus Mach number for $\beta_T = 0.5$, $\beta_U = 0$, and $\theta = 0^\circ$.

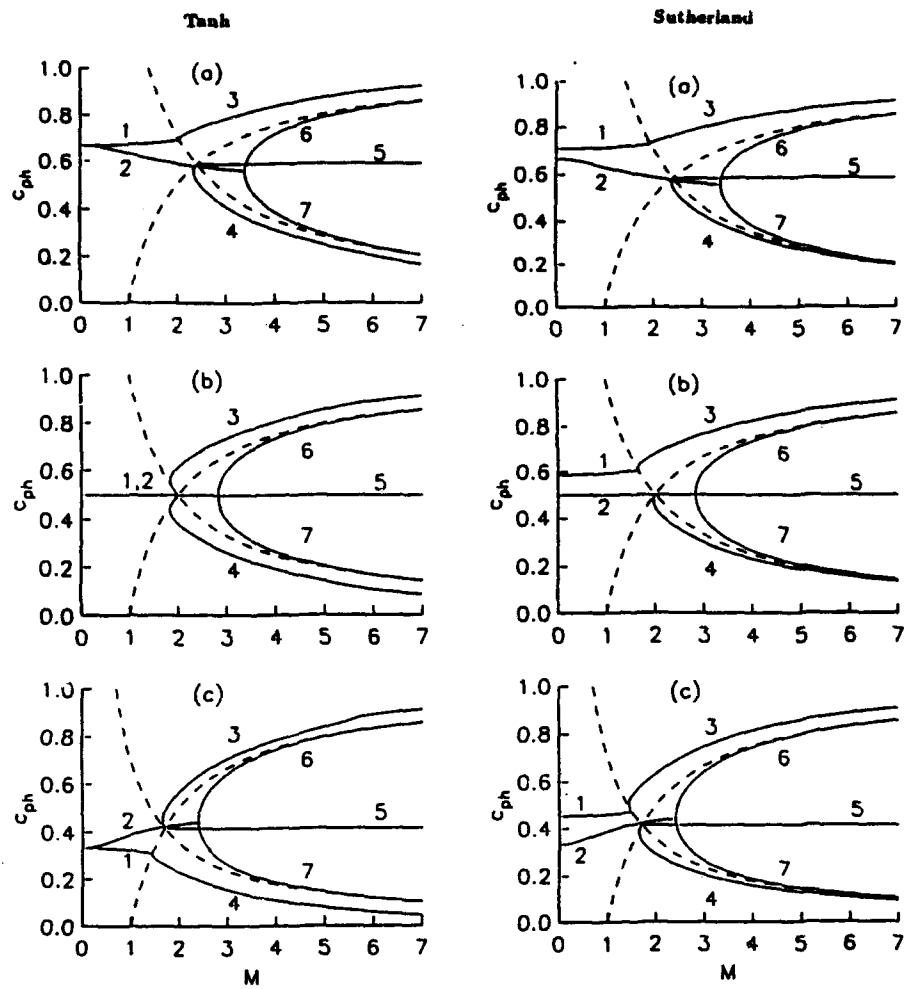


Figure 8. Plots of the neutral phase speeds as a function of Mach number for the Tanh model (left hand column) and Sutherland model (right hand column). For both $\beta_U = 0$, $\theta = 0^\circ$ and (a) $\beta_T = 2.0$, (b) $\beta_T = 1.0$, and (c) $\beta_T = 0.5$. The neutral mode classification is: (1) subsonic, $\alpha_N \neq 0$; (2) subsonic, $\alpha_N = 0$; (3) fast supersonic, $\alpha_N \neq 0$; (4) slow supersonic, $\alpha_N \neq 0$; (5) constant speed supersonic-supersonic, $\alpha_N = 0$; (6) fast supersonic-supersonic, $\alpha_N = 0$; and (7) slow supersonic-supersonic, $\alpha_N = 0$. The sonic curves are shown as dashed.

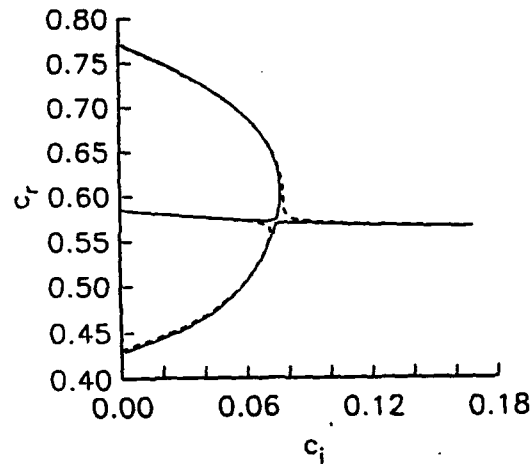
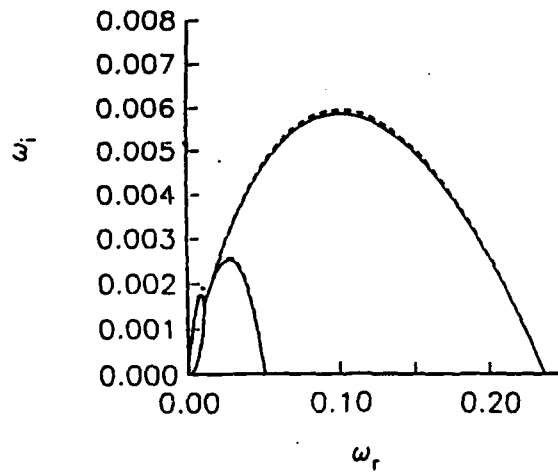


Figure 9. Plot of (a) ω_i versus ω_r and (b) c_r versus c_i with $\beta_U = 0$, $\beta_T = 2.0$ and (dashed) $M = 2.86$ and (solid) $M = 2.88$.

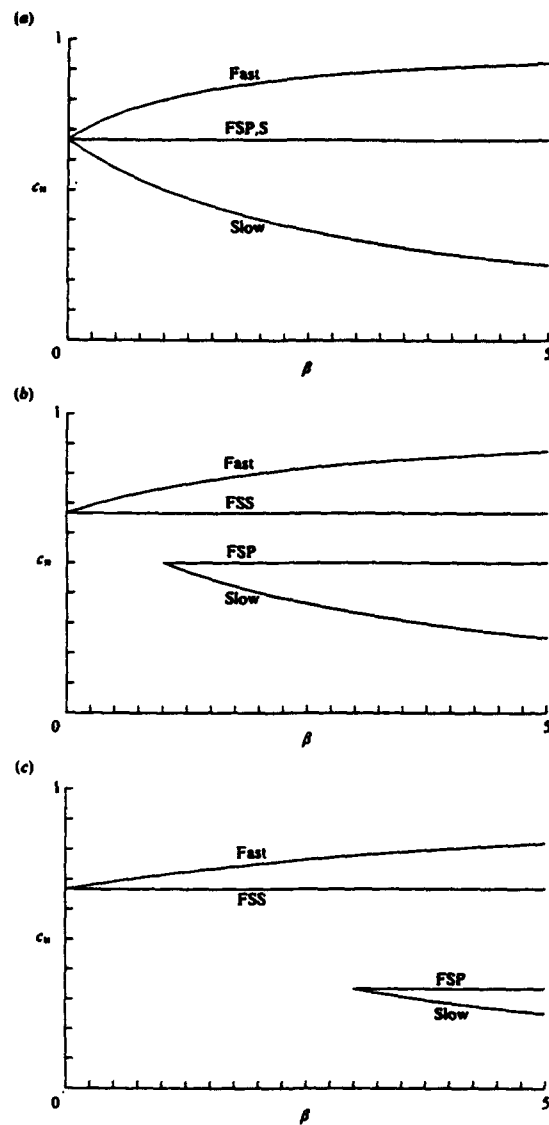


Figure 10. (a) Plot of the neutral phase speeds c_N versus β for $\beta_T = 2$, $\phi = 0.5$, and $M = 0$. (b) Plot of the neutral phase speeds c_N versus β for $\beta_T = 2$, $\phi = 1.0$, and $M = 0$. (c) Plot of the neutral phase speeds c_N versus β for $\beta_T = 2$, $\phi = 2.0$, and $M = 0$.

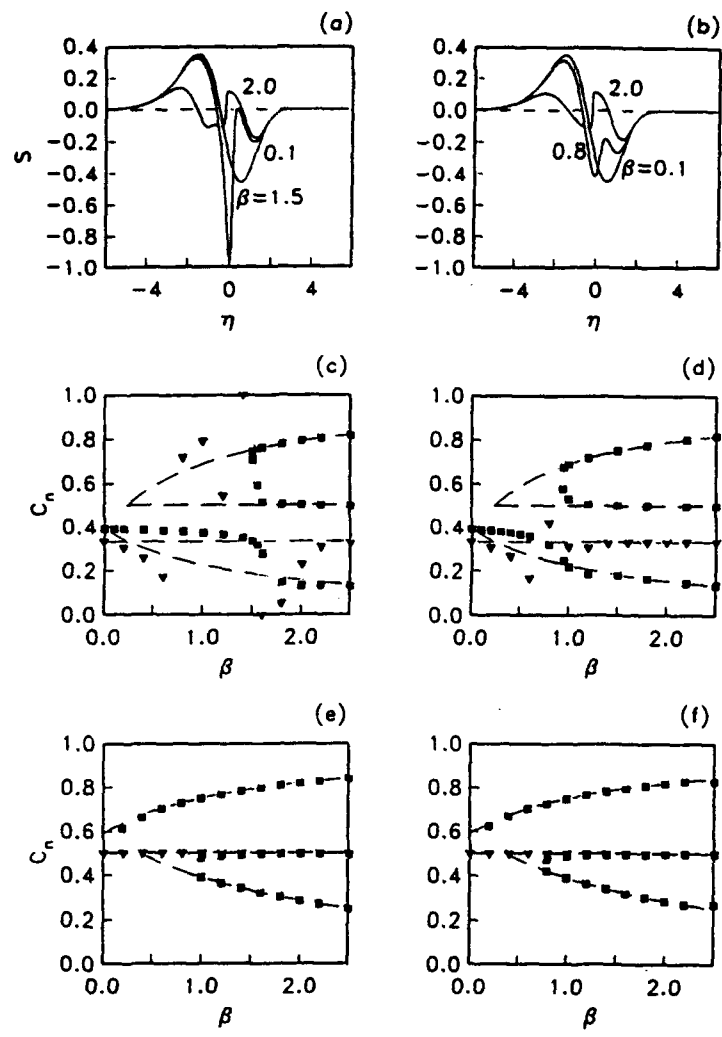


Figure 11. Plot of S versus η for various values of β , $\beta_U = 0$, $\beta_T = 0.5$, $\phi = 1$, $Ze = 20$, $M = 0$ at (a) $x = 3$ and (b) $x = 10$. Plot of neutral phase speeds versus β with $\beta_T = 0.5$ at (c) $x = 3$ and (d) $x = 10$, and with $\beta_T = 1$ at (e) $x = 3$ and (f) $x = 10$ for same parameters as (a,b). Here - - - in (c-f) denotes the neutral phase speeds obtained from the flame sheet model. The disturbances are two dimensional with $\theta = 0^\circ$. In all cases the one step irreversible Arrhenius reaction was used.

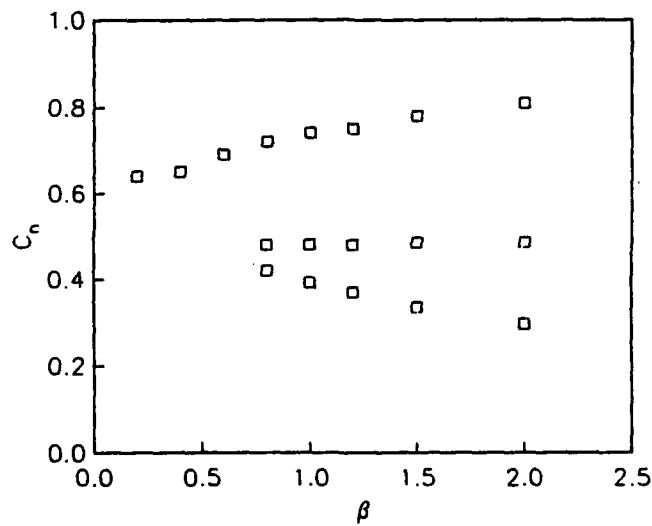
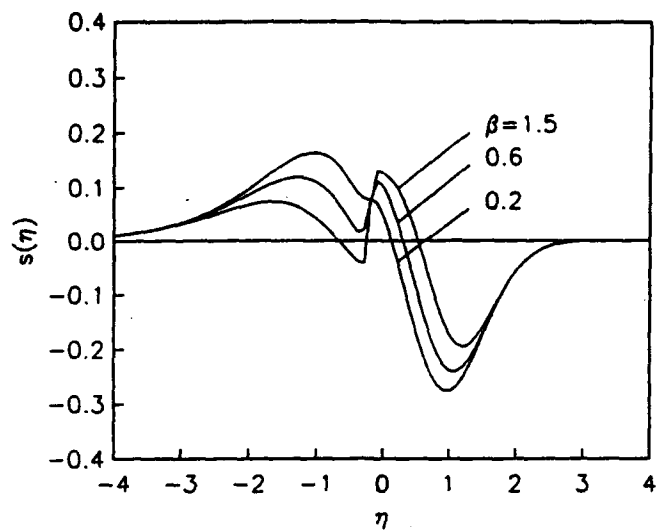


Figure 12. Plot of S versus η for various values of β , $\beta_V = 0$, $\beta_T = 1.0$, $\phi = 1$, $Ze = 20$, $M = 0$ at $x = 10$. Plot of neutral phase speeds versus β with $\beta_T = 1.0$ at $x = 10$, and with the other parameters unchanged. The disturbances are two dimensional with $\theta = 0^\circ$. In this case the Birkan and Law (1988) reaction model was used.

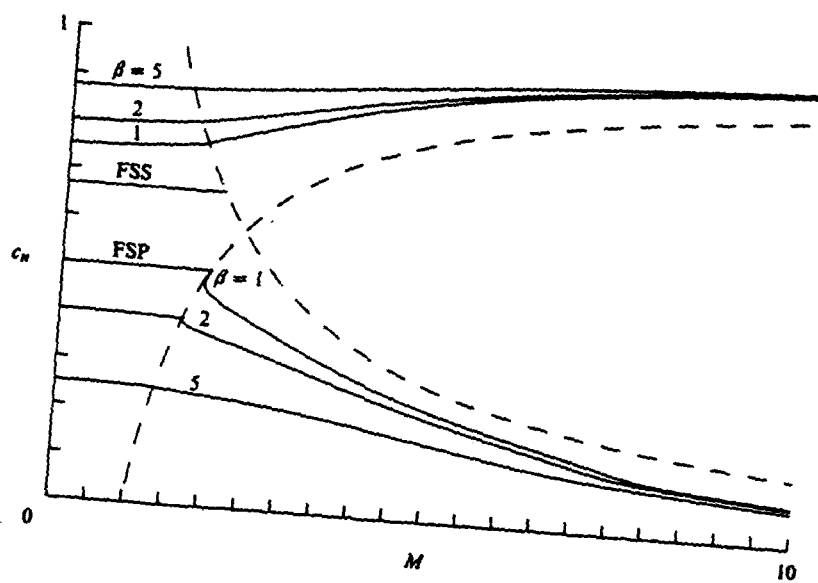


Figure 13. Plot of the neutral phase speeds (solid) and sonic speeds (dashed) versus Mach number for $\beta_T = 2$, $\beta = 1, 2, 5$, and $\phi = 1$.

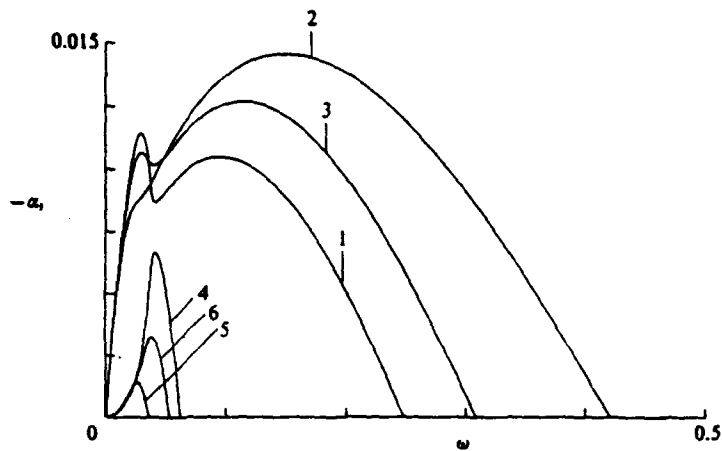


Figure 14. Plot of growth rates $-\alpha_i$ of the fast and slow two dimensional modes versus frequency for $\beta_T = 2$ and $M = 2.5$; fast modes: (1) Tanh, (2) Lock, (3) Sutherland; slow modes: (4) Tanh, (5) Lock, (6) Sutherland.

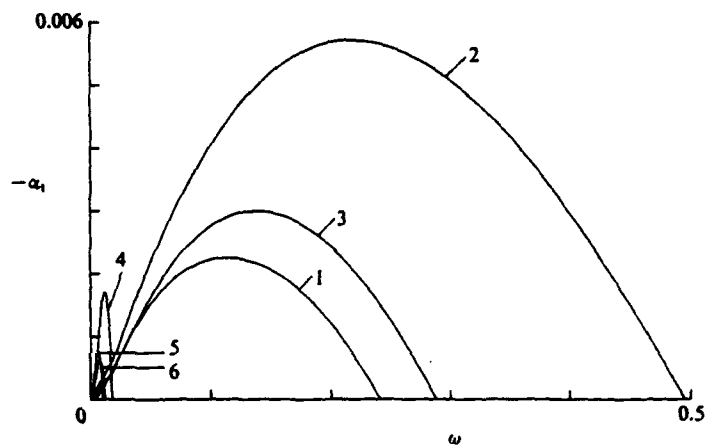


Figure 15. Plot of growth rates $-\alpha_i$ of the fast and slow two dimensional modes versus frequency for $\beta_T = 2$ and $M = 5.0$; fast modes: (1) Tanh, (2) Lock, (3) Sutherland; slow modes: (4) Tanh, (5) Lock, (6) Sutherland.

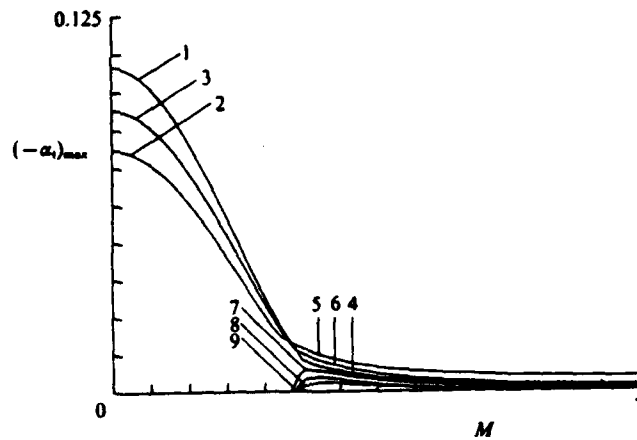


Figure 16. Plot of maximum growth rates of the two dimensional modes versus Mach number for $\beta_T = 2.0$; subsonic modes: (1) Tanh, (2) Lock, (3) Sutherland; fast modes: (4) Tanh, (5) Lock, (6) Sutherland; slow modes: (7) Tanh, (8) Lock, (9) Sutherland.

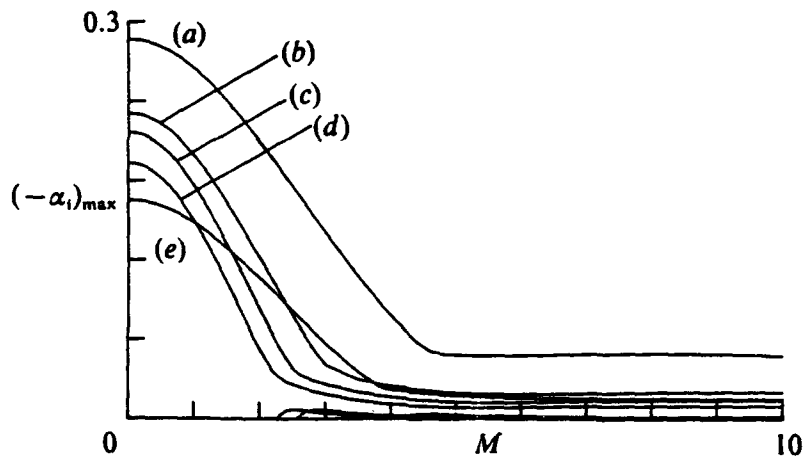


Figure 17. Plot of the maximum growth rates of the subsonic modes and their slow supersonic continuation and some fast supersonic modes versus Mach number for $\beta_T = 0.5$, $\beta_U = 0.25$, $\psi = 10^\circ$, and (a) $\theta = 80^\circ$, (b) $\theta = 60^\circ$, (c) $\theta = 45^\circ$, (d) $\theta = 0^\circ$, (e) $\theta = -45^\circ$.

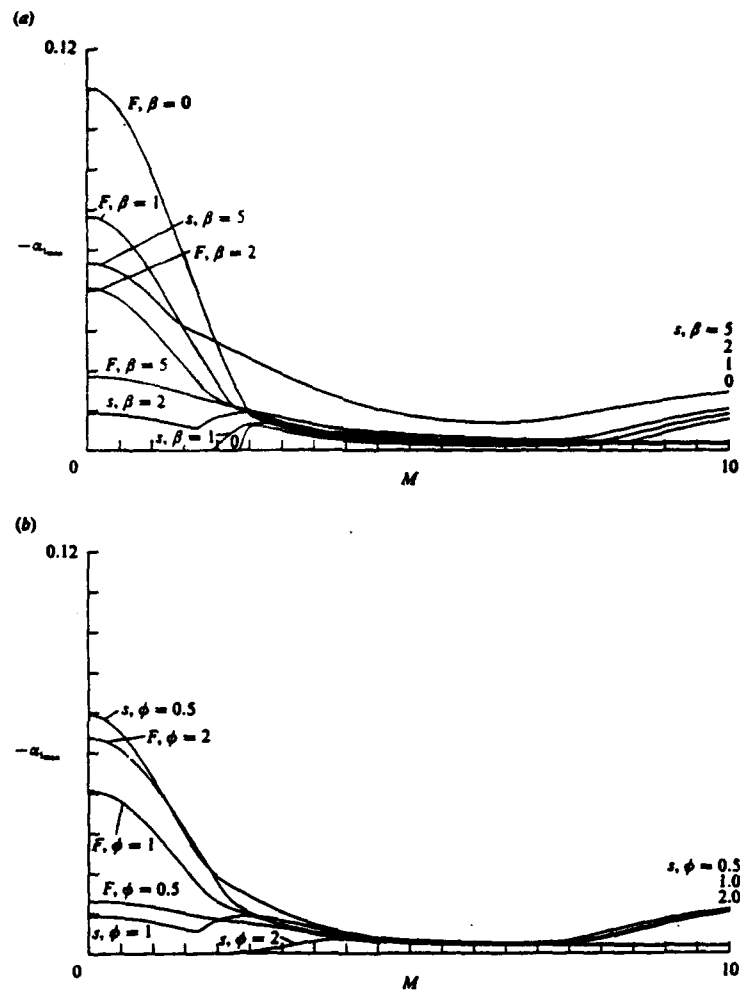


Figure 18. (a) Plot of the maximum growth rates of the fast and slow modes versus Mach number for $\beta_T = 2$, $\beta = 0, 1, 2, 5$, and $\phi = 1$. (b) Plot of the maximum growth rates of the fast and slow modes versus Mach number for $\beta_T = 2$, $\beta = 2$, and $\phi = 0.5, 1.0, 2.0$. In both, the flame sheet model was used.

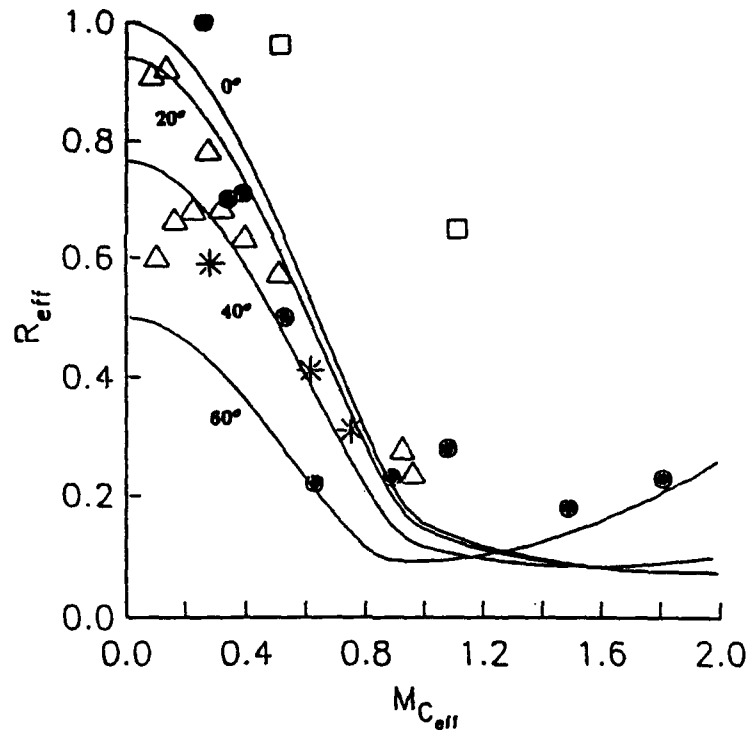


Figure 19. Plots of the normalized maximum growth rate versus the effective convective Mach number for the Tanh model with $\beta_T = 0.5$ and $\beta_U = 0$ and with $\theta = 0^\circ, 20^\circ, 40^\circ, 60^\circ$. The experimental results are the data of Papamoschou and Roshko (1988) ●; Samimy and Elliot (1990) □; Clemens and Mungal (1990) *; and Hall, Dimotakis and Rosemann (1991) Δ.

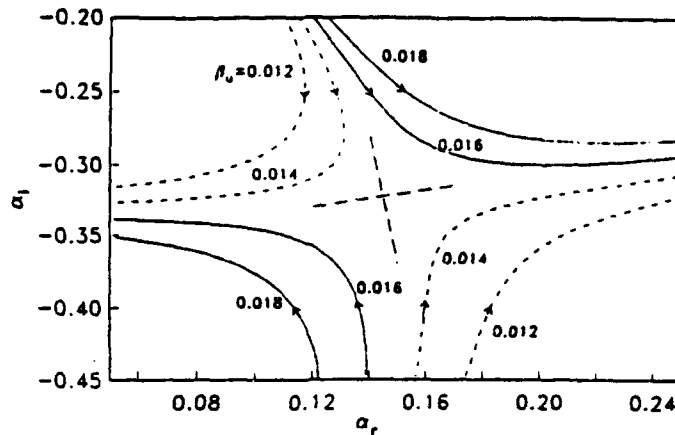


Figure 20. Plot of α_i versus α_r , as ω was varied for various values of β_U at $x = 10$ showing the saddle point. Here $\beta = 2$, $\phi = 1$, $\beta_T = 0.5$, $Ze = 20$ and $M = 0$. The mean flow was calculated using the Lock model and the one step irreversible reaction. The disturbances are two dimensional with $\theta = 0^\circ$.

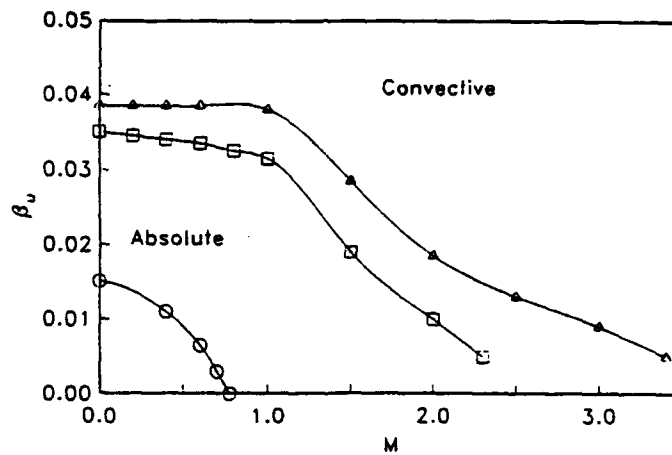


Figure 21. Transition value of β_U from absolute to convective instability for the flame sheet model as a function of M with $\phi = 1$. Results are shown for: o $\beta_T = 0.5$ and $\beta = 2$; □ $\beta_T = 0.15$ and $\beta = 2$; and △ $\beta_T = 0.15$ and $\beta = 4$. The disturbances are two dimensional with $\theta = 0^\circ$.

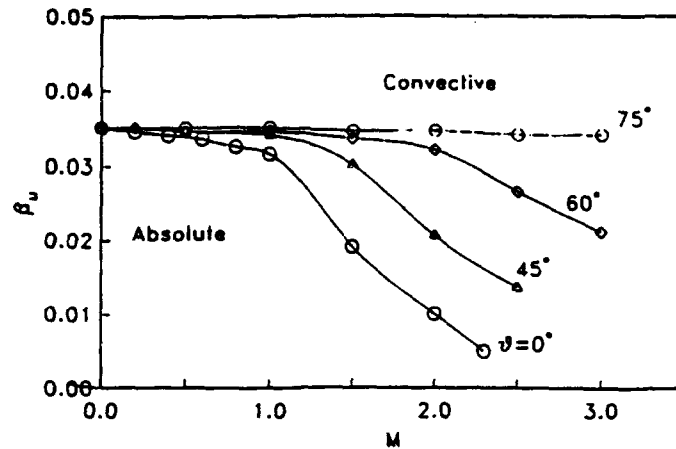


Figure 22. Transition value of β_U from absolute to convective instability for the flame sheet model as a function of M for $\phi = 1$. $\beta = 2$, $\beta_T = 0.15$ for two dimensional and oblique disturbances with $\theta = 0^\circ$, 45° , 60° , and 75° .

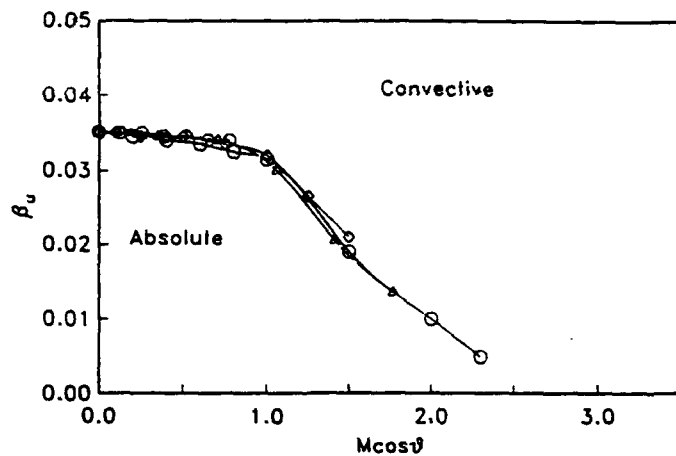


Figure 23. Transition value of β_U from absolute to convective instability for the flame sheet model as a function of $M \cos \theta$ for $\phi = 1$, $\beta = 2$, $\beta_T = 0.15$ for two dimensional and oblique disturbances with $\theta = 0^\circ$, 45° , 60° , and 75° .

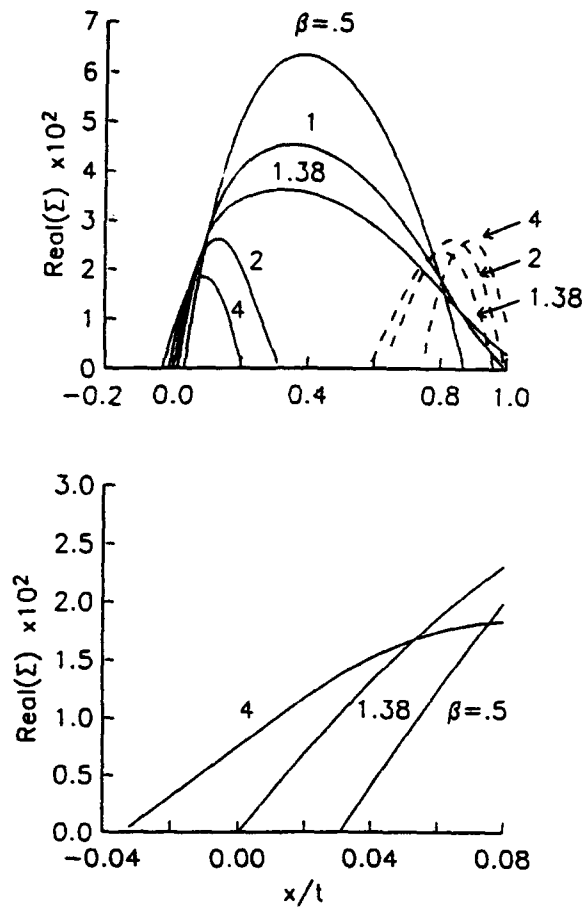


Figure 24. (a) Plot of the real part of Σ as a function of x/t for various values of β . (b) Enlargement of (a) in the region $-0.04 \leq x/t \leq 0.08$. Here $M = 0$, $\beta_T = 0.5$, $\beta_U = 0$ and $\phi = 1$. The disturbances are two dimensional with $\theta = 0^\circ$.

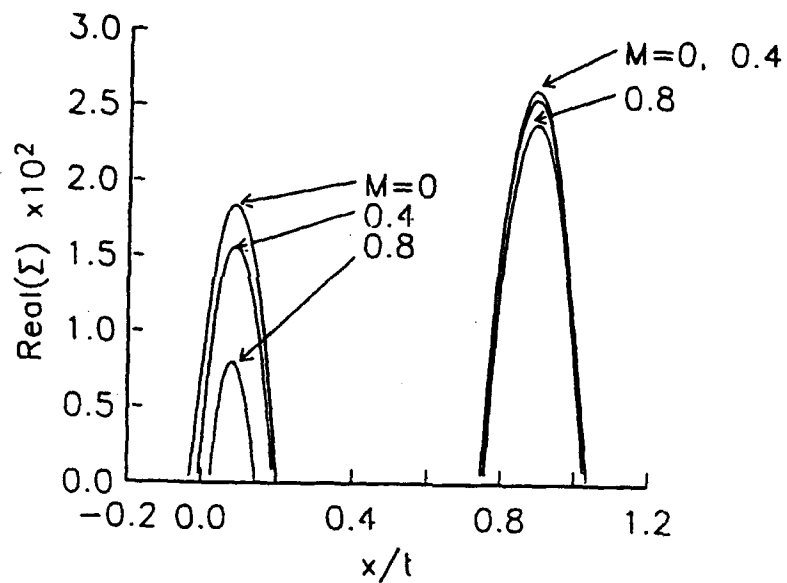


Figure 25. Plot of the real part of Σ as a function of x/t for various Mach numbers. Here $\beta = 4$, $\beta_T = 0.5$, $\beta_U = 0$ and $\phi = 1$. The disturbances are two dimensional with $\theta = 0^\circ$.

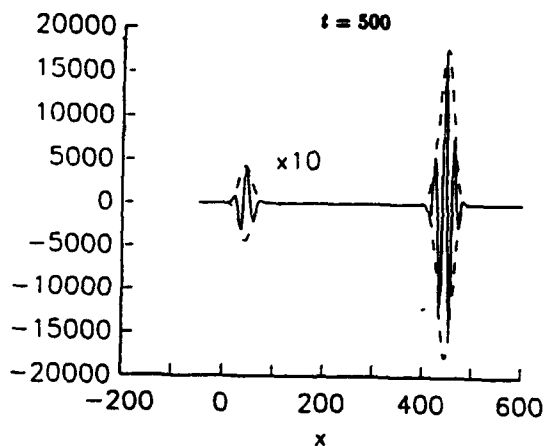
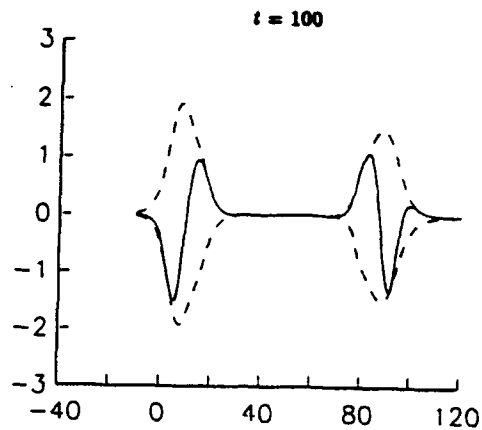


Figure 26. Plot of the wave packets and envelopes for the fast and slow modes as a function of x at (a) $t = 100$ and (b) $t = 500$. The slow packet is absolutely unstable and the fast packet convectively unstable. Here $\beta = 4$, $M = 0.4$, $\beta_T = 0.5$, $\beta_U = 0$ and $\phi = 1$. The disturbances are two dimensional with $\theta = 0^\circ$.